Journal of Medicinal Chemistry

Article

Discovery of 1-{(3R,4R)-3-[5-Chloro-2-(1-methyl-1H-pyrazol-4-ylamino)-7H-pyrrolo[2,3-d]pyrimidin-4-yloxymethyl]-4-methoxy-pyrrolidin-1-yl}propenone (PF-06459988), A Potent, WT Sparing, Irreversible Inhibitor of T790M-Containing EGFR Mutants

Hengmiao Cheng, Sajiv K Nair, Brion W. Murray, Chau Almaden, Simon Bailey, Sangita Baxi, Douglas Carl Behenna, Sujin Cho-Schultz, Deepak Dalvie, Dac M Dinh, Martin P. Edwards, Jun Li Feng, Roseanne Ferre, Ketan S Gajiwala, Michelle D Hemkens, Amy Jackson-Fisher, Mehran Jalaie, Theodore Otto Johnson, Robert S Kania, Susan Kephart, Jennifer Anne Lafontaine, Elizabeth Lunney, Kevin K. -C. Liu, Zhengyu Liu, Jean Matthews, Asako Nagata, Sherry Niessen, Martha A. Ornelas, Suvi T M Orr, Mason Pairish, Simon Planken, Shijian Ren, Daniel Tyler Richter, Kevin Ryan, Neal W Sach, Hong Shen, Tod Smeal, James Solowiej, Scott C. Sutton, Khanh Tran, Elaine Tseng, William F Vernier, Marlena Walls, Shuiwang Wang, Scott L Weinrich, Shuibo Xin, Haiwei Xu, Min-Jean Yin, Ru Zhou, Michael Zientek, and John Kath

J. Med. Chem., **Just Accepted Manuscript** • DOI: 10.1021/acs.jmedchem.5b01633 • Publication Date (Web): 12 Jan 2016

Just Accepted

ACS Publications

Journal of Medicinal Chemistry is published by the American Chemical Society. 1155 Sixteenth Street N.W., Washington, DC 20036

	Richter, Daniel; Pfizer Global Research and Development, Discovery Ryan, Kevin; Pfizer Sach, Neal; Pfizer Worldwide R&D, Medicinal Chemistry Shen, Hong; Pfizer, Chemistry Smeal, Tod; Eli Lilly and Company Solowiej, James; Pfizer Sutton, Scott; Pfizer, Inc., Cancer Chemistry Tran, Khanh; Pfizer Tseng, Elaine; Pfizer Vernier, William; Pfizer Walls, Marlena; Regulus Therapeutics Inc, Wang, Shuiwang; WuXi Apptec Weinrich, Scott; Pfizer Xin, Shuibo; WuXi App Tec Co., Shanghai, China Xu, Haiwei; WuXi Apptec Yin, Min-Jean; Pfizer Zhou, Ru; Pfizer Zientek, Michael; Pfizer, PDM Kath, John; Pfizer Global Research & Development, Worldwide Medicinal Chemistry

Discovery of 1-{(3R,4R)-3-[5-Chloro-2-(1-methyl-1H-pyrazol-4-ylamino)-7H-pyrrolo[2,3-d]pyrimidin-4-yloxymethyl]-4-methoxy-pyrrolidin-1-yl}propenone (PF-06459988), A Potent, WT Sparing, Irreversible Inhibitor of T790M-Containing EGFR Mutants

Hengmiao Cheng,*[†] Sajiv K. Nair,*[†] Brion W. Murray,*[†] Chau Almaden,[†] Simon Bailey,[†] Sangita Baxi,[†] Doug Behenna,[†] Sujin Cho-Schultz,[†] Deepak Dalvie,[†] Dac M. Dinh,[†] Martin P. Edwards,[†] Jun Li Feng,[†] Rose Ann Ferre,[†] Ketan S. Gajiwala,[†] Michelle D. Hemkens,[†] Amy Jackson-Fisher,[†] Mehran Jalaie,[†] Ted O. Johnson,[†] Robert S. Kania,[†] Susan Kephart,[†] Jennifer Lafontaine,[†] Beth Lunney,[†] Kevin K.-C. Liu,[†] Zhengyu Liu,[†] Jean Matthews,[†] Asako Nagata,[†] Sherry Niessen,[†] Martha A. Ornelas,[†] Suvi T. M. Orr,[†] Mason Pairish,[†] Simon Planken,[†] Shijian Ren,[≠] Daniel Richter,[†] Kevin Ryan,[†] Neal Sach,[†] Hong Shen,[†] Tod Smeal,[†] Jim Solowiej,[†] Scott Sutton,[†] Khanh Tran,[†] Elaine Tseng,[†] William Vernier,[†] Marlena Walls,[†] Shuiwang Wang,[≠] Scott L. Weinrich,[†] Shuibo Xin,[≠] Haiwei Xu,[≠] Min-Jean Yin,[†] Michael Zientek,[†] Ru Zhou,[†] and John C. Kath[†]

[†]La Jolla Laboratories, Pfizer Worldwide Research and Development, 10770 Science Center Drive, San Diego, California 92121, United States

[≠]Wuxi AppTec, 288 Fute Zhong Road, Waigaoqiao Free Trade Zone, Shanghai 200131, China

Abstract: First generation EGFR TKIs (gefitinib, erlotinib) provide significant clinical benefit for NSCLC cancer patients with oncogenic EGFR mutations. Ultimately, these patients disease progresses, often driven by a second-site mutation in the EGFR kinase domain (T790M). Another liability of the first generation drugs is severe adverse events driven by inhibition of WT EGFR. As such, our goal was to develop a highly potent irreversible inhibitor with the largest selectivity ratio between the drug-resistant double mutants (L858R/T790M, Del/T790M) and WT EGFR. A unique approach to develop covalent inhibitors, optimization of *reversible binding affinity*, served as a cornerstone of this effort. PF-06459988, was discovered as a novel, third generation irreversible inhibitor, which demonstrates (i) high potency and specificity to the T790M-containing double mutant EGFRs, (ii) minimal intrinsic chemical reactivity of the electrophilic warhead, (iii) greatly reduced proteome reactivity relative to earlier irreversible EGFR inhibitors and (iv) minimal activity against WT EGFR.

INTRODUCTION

Lung cancer is the leading cause of cancer-related death worldwide, with an estimated over 1 million new cases diagnosed and over 1 million deaths each year.[1] In non-small cell lung cancer (NSCLC) which accounts for 85% of lung cancer, patients harboring mutations in EGFR constitute between 10-30% of the overall patient population. Two frequent and mutually-exclusive primary mutations occur either in the activation loop as a point mutation (EGFR L858R) or by short deletion in exon 19 (EGFR-Del), together accounting for approximately 85 % of all cases.[2] These somatic EGFR mutants enable constitutive activation and are strong predictive biomarkers of response to first generation EGFR TKIs (gefitinib[3] and erlotinib[4]) (Figure 1). In contrast, these drugs are dose-limited by potent inhibition of their originally intended target wild type (WT) EGFR, which causes epithelium-based toxicities by blocking its role in normal adult physiology.[5,6] Treatment of EGFR-mutant NSCLC patients with the first generation EGFR TKIs provides excellent response rates and disease control for 11 to 14 months, but patients invariably become resistant to these therapies and their disease progresses. Of the drug-resistant EGFR-mutant NSCLC patients, approximately 60% harbor an additional mutation in the EGFR kinase domain (T790M) in *cis* with the primary activating mutation[7] that renders the receptor insensitive to inhibition by the EGFR TKIs, and thus, restoring constitutive EGFR signaling. The resistance mechanism derived from T790M mutation is believed to come from a number of components, including the increased ATP binding affinity for T790M mutants, the steric clash between the Met790 gatekeeper side chain and the aniline moiety that is utilized by the first generation EGFR TKIs to bind in the kinase back-pocket and the altered catalytic domain conformation.[8,9,10]

The first generation of EGFR drugs relied on reversible affinity to achieve potency. More recently, a covalent inhibition strategy has been used because it delivers distinct pharmacological properties. Irreversible kinase inhibitors can achieve advantages over reversible compounds by delivering complete and sustained target engagement in the presence of high intracellular concentrations of ATP in the cells, and by requiring the physical turnover of kinase proteins to restore inhibited signaling pathways.[11,12,13] Indeed, second generation, irreversible inhibitors of EGFR WT (canertinib (CI-1033)[14]; dacomitinib[15]; afatinib[16]) (Figure 1) which covalently modify EGFR Cys797 demonstrate increased cellular potency against T790M mutants relative to their reversible counterparts . However, because these compounds maintain the aniline moiety that clashes with Met790 side chain, their T790M activity is less than their activity against the primary activating EGFR mutants. As a result, their clinical efficacy to treat T790M patients is limited due to dose-limiting toxicity associated with inhibition of WT EGFR.

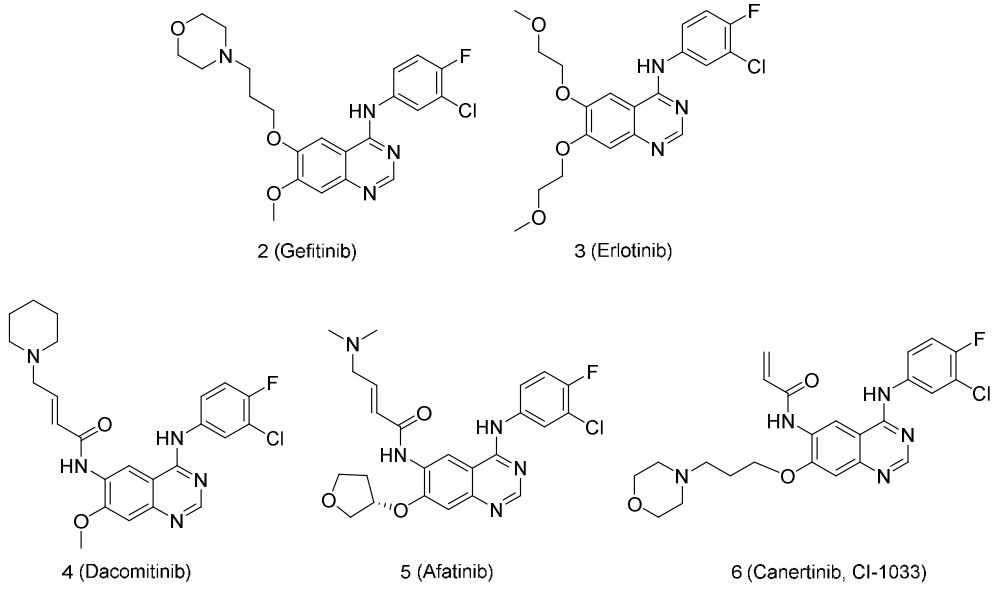

Figure 1. Summary of 1st generation and 2nd generation EGFR inhibitors.

In response to this unmet need, and because irreversible inhibitors demonstrated better potency against EGFR T790M mutants than reversible inhibitors, an effort was initiated to discover highly potent irreversible inhibitors of the drug resistant T790M mutants that spare EGFR WT activity to the greatest extent as a means to minimize mechanism-based toxicities. Others have pursued irreversible inhibitors of EGFR T790M, resulting in the identification of WZ-4002[17] (**7**), rociletinib[18] (CO-1686, **8**) and osimertinib[19,20,21] (AZD9291, **9**) (Figure 2). Both rociletinib and osimertinib have progressed to advanced clinical trials. In addition, there are several recent publications discussing the design and SAR for novel third generation irreversible EGFR inhibitors.[22,23,24,25,26] The discovery of 1-{(3R,4R)-3-[5-Chloro-2-(1-methyl-1H-pyrazol-4-ylamino)-7H-pyrrolo[2,3-d]pyrimidin-4-yloxymethyl]-4-methoxy-pyrrolidin-1-yl}propenone (PF-06459988, **1**)[27,28], a highly potent inhibitor of EGFR T790M with unprecedented selectivity over EGFR WT, is described in this manuscript.

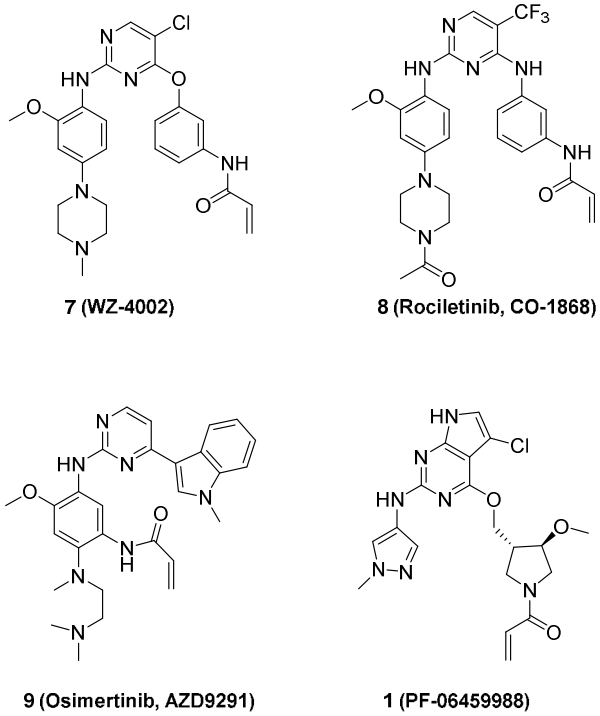

Figure 2. Summary of 3rd generation EGFR inhibitors.

RESULTS AND DISCUSSION

Objective.

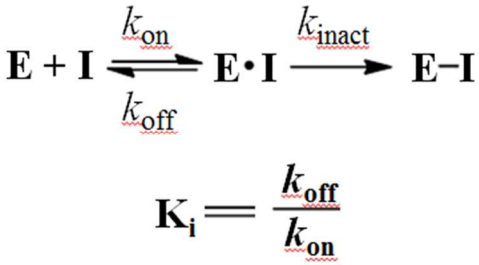

Figure 3. Kinetic mechanism for two-step covalent inhibition of EGFR.

The inactivation of EGFR occurs through a two-step process that begins with reversible binding to EGFR followed by covalent bond formation with the thiol of Cys797 to form a covalent adduct (Figure 3). Therefore, irreversible inhibitor potency can be increased by maximizing the reversible binding affinity (K_i=k_{off}/k_{on}), the specific reactivity (k_{inact}), or the inherent chemical reactivity of the electrophile. In addition to optimizing T790M potency and selectivity over WT, an equally significant emphasis was placed on reducing warhead reactivity to minimize proteome-wide reactivity and decrease the probability of idiosyncratic toxicity. To achieve these multiple objectives, a key strategy was to optimize the potency of inhibitors based on their reversible (non-covalent) binding affinity to EGFR T790M as opposed to the chemical reactivity of the warhead. To effectively carry out this strategy, a high capacity binding kinetics assay was developed which is capable of separating the reversible binding affinity from the inactivation rate. Typically, irreversible kinetic analysis to determine reversible affinity (K_i), and specific reactivity k_{inact} is low throughput and labor intensive. However, to truly leverage binding affinity

SAR it was essential to be able to test all new inhibitors on a weekly basis. To do so, a high throughput irreversible kinetics screening assay capable of coarsely defining reversible binding affinity (K_i^{est}) and overall irreversible inactivation (k_{obs}/I) was developed. Specialized reaction conditions were used to enhance the predictability of this method.[29,30,31] Since an inhibitor's inactivation rate is governed by a pseudo-second-order rate constant (k_{inact}/K_i), it is highly dependent on the inhibitor concentration and its chemical properties. It was recognized that in any given week a range of inhibitors would be tested from weak binders to highly optimized inhibitors. To address this issue, five inhibitor concentrations (0.01, 0.05, 0.1, 1 and 5 μM) were selected to ensure at least one or two are in the proper range to measure the initial reversible binding event (between 25-80% inhibition of the initial linear (60-120 sec) portion of the inactivation time-course). When the initial region of the inactivation time course is linear, then the dominant contribution to inhibition is reversible binding affinity. Placing a constraint on the observed percent inhibition (25-80%) kept the measurement in an accurate region; enough inhibition to be confident in the binding affinity but not too much that there is a large contribution from reactivity or too slow of an enzymatic rate to be accurate. The full inactivation time course for a given inhibitor concentration is defined by a rate constant (k_{obs}). To normalize the contribution of the inhibitor concentration to the observed inactivation rate, it is divided by the inhibitor concentration (k_{obs}/I). This value encompasses contributions from both reversible binding affinity and chemical reactivity. Under the assay conditions, k_{obs}/I is correlated to k_{inact}/K_i. To determine the correlation between K_i^{est} and K_i, both established and absolute values were generated for a structurally diverse set of compounds using the L858R/T790M enzyme (Figure 4). The correlation between these values supported the use of K_i^{est} for inhibitor design.

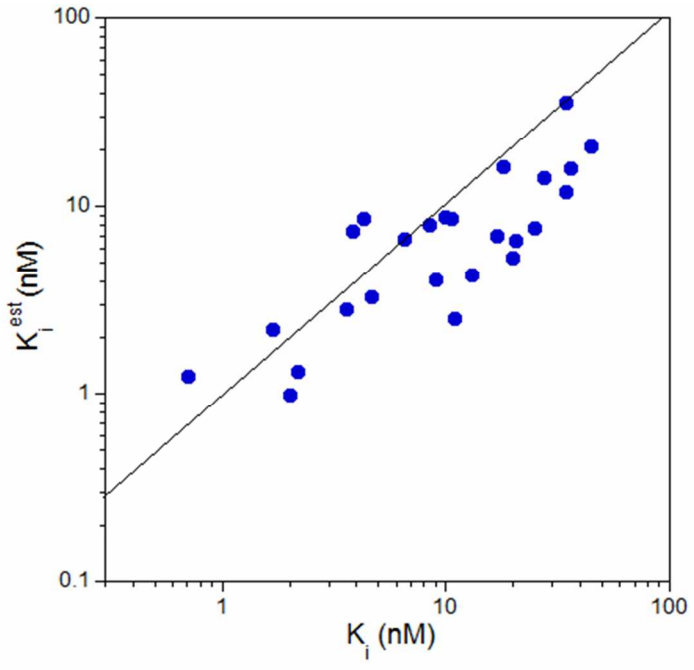

Figure 4. Correlation between absolute and estimated K_i values, $R^2 = 0.68$.

The irreversible screening assay provides two important pieces of data from an appropriate progression curve; *1)* the percent inhibition value at the drug concentration used to generate that curve which provides the K_i^{est} and *2)* the k_{obs}/I value (which is proportional to k_{inact}/K_i) from that same progression curve which provides a measure of enzyme inactivation. The assay consistently provided data for multiple compounds each week (medium number of compounds per week = 14; maximum number of compounds run in one week = 91) and became the primary assay used throughout the duration of the program.

The irreversible screening assay was supplemented with two additional assays to round out the set of primary screens used to fully characterize irreversible inhibitor SAR. To further assist in minimizing warhead reactivity, a glutathione (GSH) conjugation assay was developed which monitored parent compound loss in the presence of GSH to establish a half-life.[29] Canertinib was used as a control, and the half-lives of test compounds were normalized to that of canertinib

($t_{1/2}$ *ca:* 21 min); to describe the intrinsic chemical reactivity of the warhead. To drive toward the critical objective of achieving the high levels of selectivity for EGFR T790M over EGFR WT a pair of cellular ELISA assays were used which measure the ability of a compound to inhibit phosphorylation of EGFR L858R/T790M (H1975 cells) relative to EGFR WT (A549 cells).

Establishing Early Leads

The critical structural difference in the surface of the ATP binding pocket between EGFR WT and the T790M mutant resides at the gatekeeper residue. This mutation changes the amino acid residue from the polar threonine to a non-polar methionine. Therefore, to attain the largest difference in potency between EGFR T790M and EGFR WT, optimizing hydrophobic interactions between an inhibitor and the Met790 side chain may provide high levels of T790M potency and selectivity. Modeling studies indicated that the pyrrole portion of a pyrrolopyrimidine (PP) core would achieve effective hydrophobic interactions with the Met790 side chain and provide an additional hydrogen bond interaction with the backbone carbonyl of Gln791 (Figure 5).

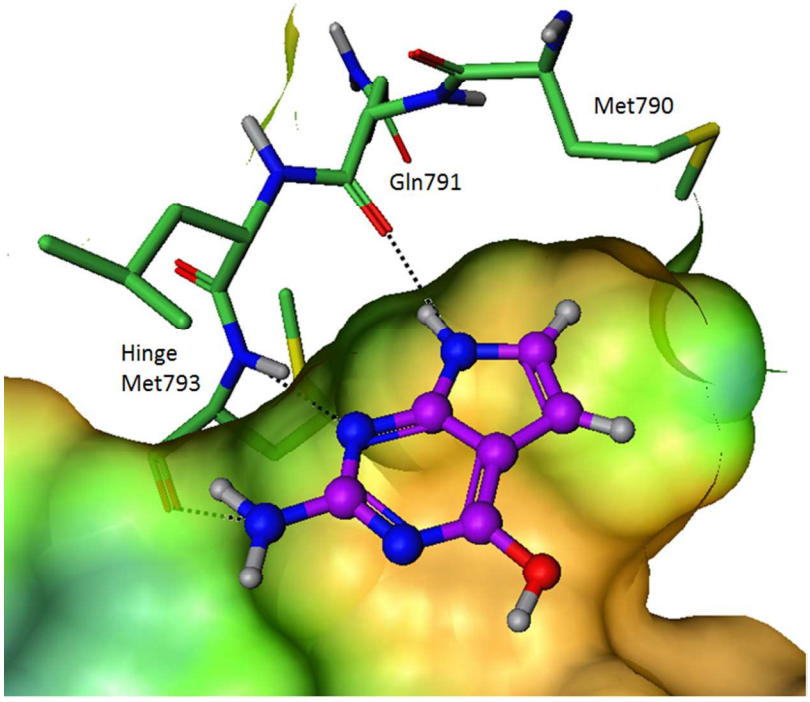

Figure 5. Modeled interactions of PP core with Met790 and hinge residue of monomeric L858R/T790M EGFR. Hydrophobic surface of the binding site near the hinge and T790M is shown.

Initial designs with the PP core led to the identification of an early lead, compound **10** (Figure 6). This compound had a high binding affinity to the L858R/T790M double mutant (DM) with a K_i^{est} of 2 nM (43% inhibition at 0.05 μM), and a substantial inactivation rate with k_{obs}/I of 51,300 $M^{-1}s^{-1}$. The k_{obs}/I value was obtained at 0.05 μM inhibitor concentration. The substantial inactivation rate for **10** was confirmed by the measured k_{inact}/K_i rate of 59,123,000 $M^{-1}s^{-1}$. Compound **10** was an attractive lead, potently inhibiting EGFR L858R/T790M autophosphorylation (IC_{50} = 4 nM) in the H1975 cell line but only modestly inhibiting EGFR WT autophosphorylation (IC_{50} = 0.79 μM) in the A549 cell line. Relative to benchmark compound canertinib in a glutathione conjugation assay, compound **10** exhibits a 6-fold reduction in intrinsic chemical reactivity with thiol nucleophiles.

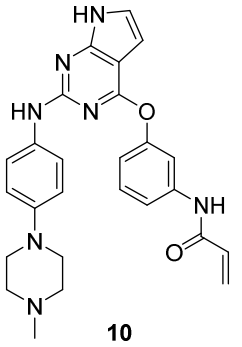

10

K_i^{est} (DM): 2 nM
k_{obs}/I: 51,300 $M^{-1}s^{-1}$
H1975 pEGFR IC_{50}: 4 nM
A540 pEGFR IC_{50}: 0.79 μM

Figure 6. Summary of key *in vitro* potency and WT selectivity data for **10**.

Using our crystallography platform[32] we obtained a cocrystal structure of **10** with monomeric EGFR L858R/T790M (Figure 7a). The 1.5 Å ligand-protein complex shows covalent modification of the target residue Cys797 *via* the Michael acceptor of the ligand. The enzyme is in a unique conformation for EGFR relative to previous structures with respect to the Asp855-Phe856-Gly857 (DFG) motif and the activation loop conformation. While the Phe856 side chain is oriented out of the hydrophobic core of the protein, partially occupying the ATP binding site, the Asp855 side chain is positioned into the hydrophobic core in a DFG-out conformation. The conformation of the rest of the activation loop is nearly identical to that in the active EGFR kinase domain. There is an approximately 20 degree rotation of the N-lobe relative to the C-lobe when compared with the apo-protein structure (Figure 7b) requiring unwinding of the first turn of the αC-helix in the ligand-bound structure.

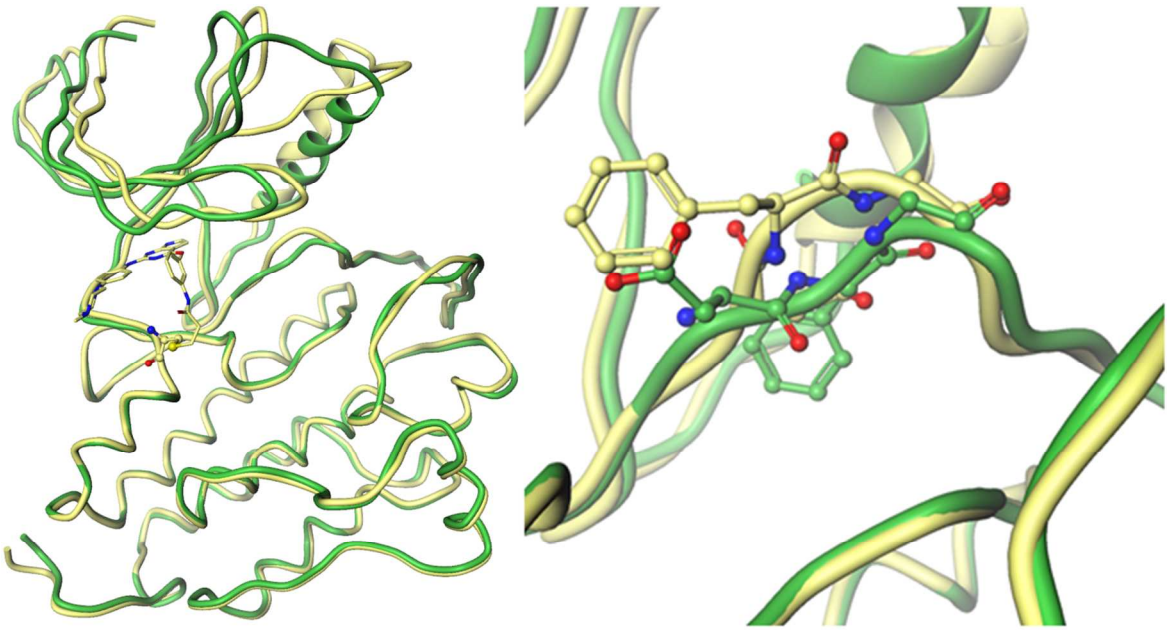

Figure 7a. Monomeric L858R+T790M ligand bound conformation (yellow) *vs*. EGFR WT active (green). A classic DFG out conformation is observed in the ligand bound T790M structure, however the activation loop is in a state nearly identical to the active form. The Phe856 side chain is oriented out of the protein core, partially occupying the ATP binding site, and the Asp855 side chain is positioned into the hydrophobic core.

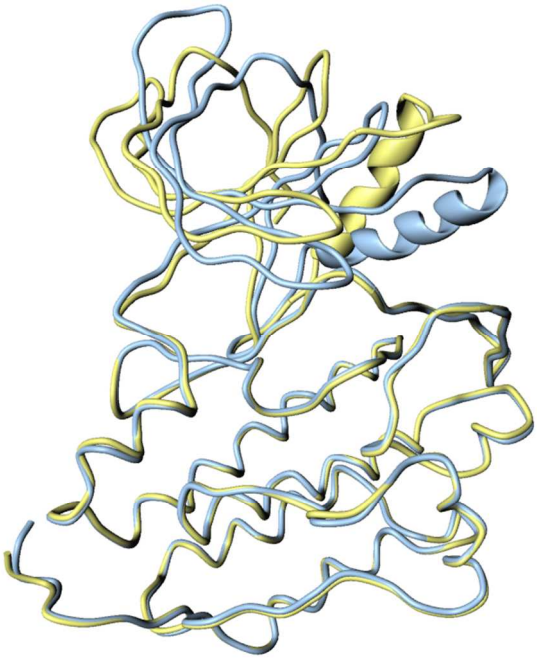

Figure 7b. Comparison of the monomeric L858R+T790M protein conformations in the apo (blue) and the ligand bound (yellow) states. Rotation of the N-lobe and α-C helix occurs on ligand binding.

The cocrystal structure suggests that the binding affinity of **10** is achieved through specific and non-specific interactions with the protein independent of the covalent bond formation with Cys797 (Figure 8). The PP core establishes specific donor-acceptor-donor interactions with the backbone atoms of hinge residues 791 – 793. The phenoxy linker occupies the ATP-sugar binding site and forms a van der Waals interaction with Phe856 from the DFG motif. The G-loop is well ordered with the Phe723 side chain turned inward toward the ligand binding site to make van der Waals contact with Phe856. The phenyl ring of the phenylpiperazine group is engaged in van der Waals interactions with hinge residues 794 – 796, whilst the piperazine ring projects into the solvent region without any visible specific interactions with the protein. Two key water interactions are observed; one between nitrogen of the ligand's propionamide group, the backbone atom of the Arg841 and the side chain carbonyl of the Asn842, and a second between the carbonyl of the acrylamide and the backbone of Cys797. The side chain of the mutated gatekeeper residue Met790 forms hydrophobic interactions with the pyrrole of the PP core (distance between the beta carbon of Met790 and the C2 carbon atom of the pyrrole ring is 3.7 Å). In contrast, when this same ligand is modeled in the WT enzyme the C2 atom of the pyrrole comes within 2.7 Å of the hydroxyl group of the gatekeeper Thr790 residue (The modeling result is discussed in the supporting information section). This unfavorable interaction is the presumed origin of the high selectivity for drug-resistant T790M mutant EGFR over WT.

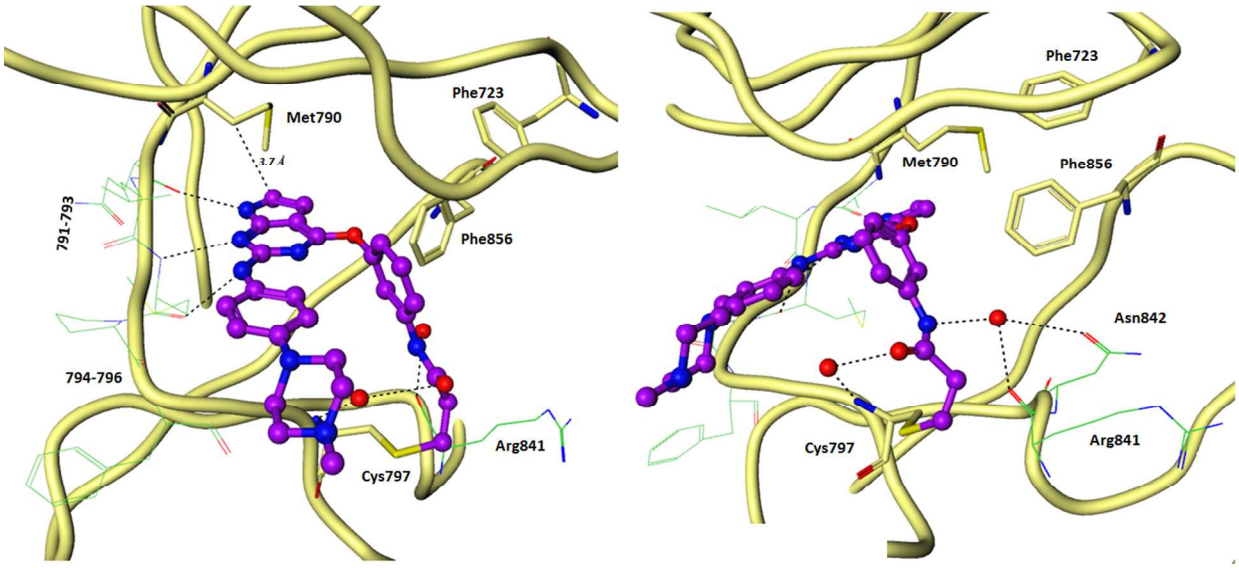

Figure 8. Compound **10** complex with monomeric L858R+T790M KD (1.5 Å). Two views are shown. Hydrogen bonds to the hinge are shown, with key protein residues highlighted in stick form. Some parts of the protein are omitted for clarity. Clear covalent modification of Cys797 is observed. The ligand phenoxy group interacts with Phe856 through VDW interactions. Two key waters are also highlighted (red spheres).

An edge-face π-interaction exists between the phenyl rings of the anilinopiperazine and the phenoxy linker which may assist in optimally positioning the acrylamide warhead to enable reaction with Cys797.

Next, the primary liabilities of **10** were addressed, specifically poor permeability (RRCK[33,34] $2x10^{-6}$cm/sec), potent dofetilide binding activity (IC_{50}=1 μM) and high clogP (4.6). The highly basic 4-piperazinyl–aniline was thought to play a significant role in these liabilities. Replacement of the aniline with an amino-pyrazole isostere was envisioned to provide a less lipophilic, metabolically stable surrogate which (unlike the aniline) would be less prone to reactive metabolite formation.[35] Furthermore, the lower lipophilicity of an amino-pyrazole functionality might enable removal of the basic amine found in the piperazinyl-aniline resulting

in a more ligand-efficient lead. To investigate this possibility, the N1-methyl-3-amino- and N1-methyl-4-amino-pyrazoles **11** and **12** were prepared (Table 1). Both compounds demonstrated increased permeability and decreased dofetilide binding activity relative to **10** while maintaining good EGFR L858R/T790M potency and selectivity over EGFR WT (>100-fold). Ligand efficiency (LE, calculated from K_i^{est}) for **11** and **12** are 0.41 and 0.45, respectively, which are significantly higher than LE of 0.37 for **10**. The 4-amino-pyrazole **12** better matched the EGFR T790M binding affinity, inactivation rate (k_{obs}/I), cellular potency and intrinsic chemical reactivity to GSH of **10** but showed increased microsomal clearance relative to **10** and **11**.

Table 1. Summary of Early Leads.

Compound ID	Structure	K_i^{est} (nM)	k_{obs}/I $M^{-1}s^{-1}$	H1975 IC_{50} (nM)	A549 IC_{50} (μM)	WT/ DM	LogD[a]	clogP	HLM Cl[b] (μL/ min/ g)	RRCK[c] (10^{-6} cm/sec)	GSH $T_{1/2}$ relative to canertinib[d]
10	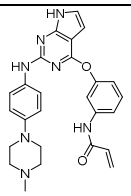	2	51,300 (at 0.05 μM)[e]	4	0.79	198	2.7	4.6	20	2	6
11	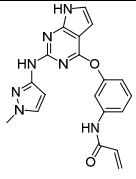	14	4,080 (at 1 μM)[e]	27	7.6	281	3.0	2.7	11	10	4

12	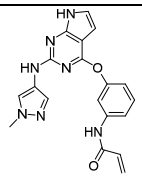	3	37,500 (at 0.05 μM) [e]	13	1.6	123	3.2	2.7	66	7	7

[a]log *D* was measured at pH 7.4. [b]Human liver microsomal intrinsic clearance. [c]Permeability measured with low-efflux MDCKII cell. [d]Chemical reactivity of warhead with glutathione relative to canertinib at pH 7.4. [e]Inhibitor concentration at which the k_{obs}/I is calculated.

The 1.4 Å co-crystal structure of **12** (Figure 9) is similar to that of **10,** with the pyrazole making a similar edge-face interaction with the phenyl ether bearing the warhead. The two C-H bonds on the pyrazole ring in **12** are polarized and the C-H at the 3-position of the pyrazole forms a weak non-classical H bond with the backbone carbonyl of Met793 in the hinge. The lower binding affinity of the 3-aminopyrazole **11** can be explained by the unfavorable interaction between the pyrazole 2-N and the backbone carbonyl of M793 in an orientation that maintains the edge-face interaction between the pyrazole and phenyl ether.

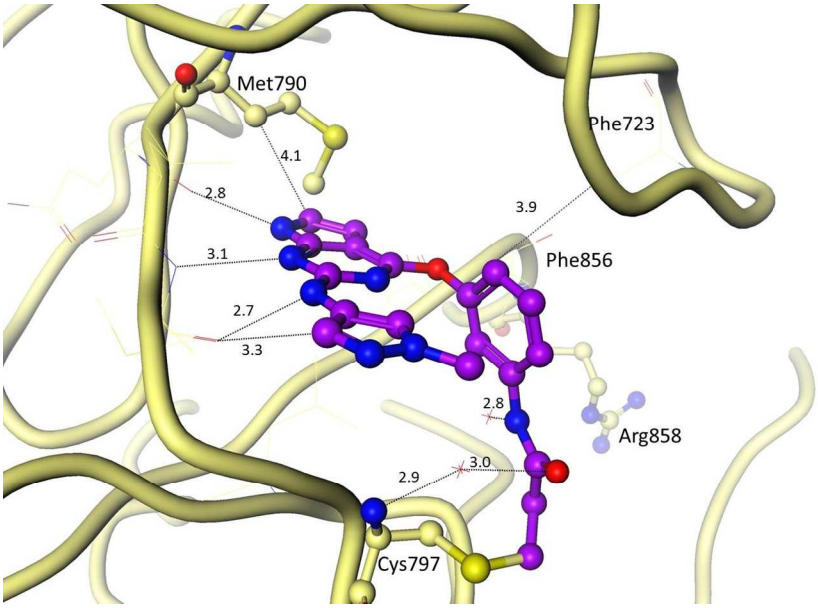

Figure 9. Compound **12** binding interactions with the monomeric EGFR L858R/T790M binding site.

Having established the N-methyl-4-aminopyrazole as a suitable isostere for the 4-piperazinyl-aniline, the linker region of the molecule was optimized as a means to reduce metabolic clearance and further minimize the reactivity of the warhead.

Aliphatic Linkers to Minimize Warhead Reactivity.

The intrinsic chemical reactivity of a warhead is influenced by the electronic properties of the linker, in this case the aromatic ring from which the warhead is connected. In order to mitigate the potential of forming off-target covalent adducts, the design strategy was to minimize the warhead's reactivity by avoiding electron deficient linking motifs. It was predicted that utilizing *aliphatic* linkers would remove the conjugative effects of aromatic systems (e.g. phenoxy linker of **12**, anilide of canertinib) on the warhead and afford reduced reactivity. A 3-pyrrolidinemethyl ether linker was identified to have the appropriate length, orientation and conformational

constraint[36] to position the warhead for a reaction with Cys797. Compound **13** (Table 2) was synthesized and tested, however, the K_i^{est} of 590 nM and negligible irreversible inactivation (k_{obs}/I of 830 $M^{-1}s^{-1}$ at 1 μM) indicated that significant optimization was required.

To increase binding affinity, a small hydrophobic pocket (identified from the co-crystal structure of **12**) under the G-loop, created by residues Phe723 and Val726 was targeted. Modelling of **13** (using the protein structure of **12** cocrystal structure) suggested that a small lipophilic group at the pyrrolidine 4 position would be suited (Figure 10), thus a CF_3 group was installed (chosen for metabolic stability benefits over methyl or ethyl) resulting in compound **14** (Table 2). This molecule provided a 17-fold increase in potency (K_i^{est} 35 nM) and an increase in irreversible activation (k_{obs}/I of 5410 $M^{-1}s^{-1}$ at 1 μM) relative to **13**. However, introduction of the CF_3 group was concomitant with higher intrinsic reactivity compared to other aliphatic linkers tested with the intrinsic reactivity of **14** relative to canertinib (9x) similar to that observed with **12** (7x). In order to improve the potency of the aliphatic linker compounds, alternative opportunities were sought to increase binding affinity using pyrrolidine substituents that do not increase the intrinsic reactivity.

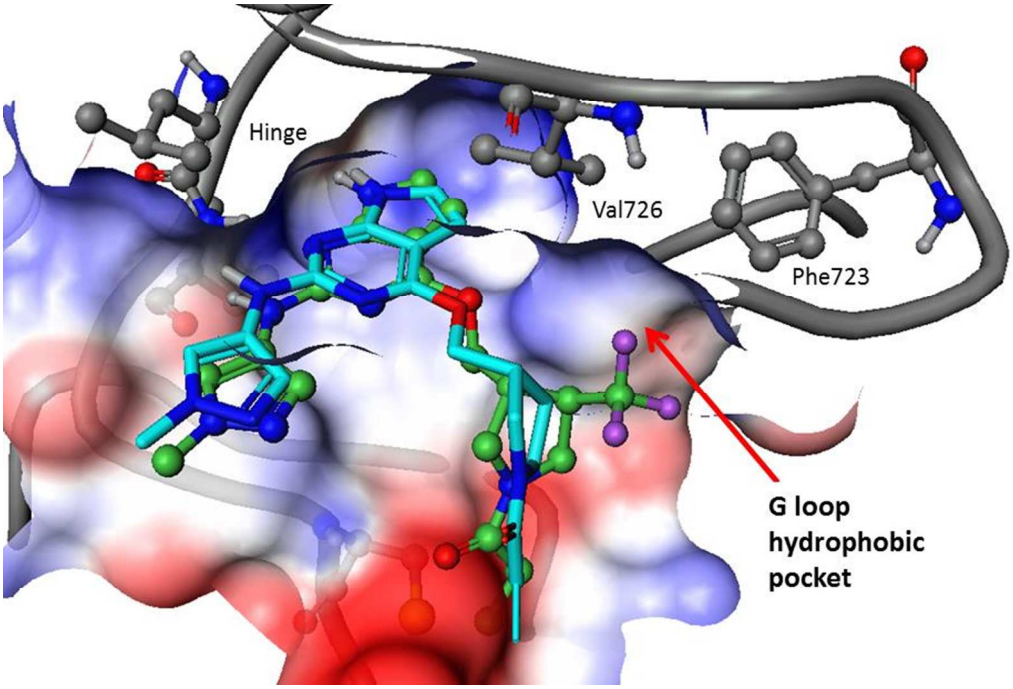

Figure 10. Comparison of modeled binding mode of **13** (stick, in blue color) in monomeric L858R/T790M EGFR and bound conformation of **14** (ball and stick, in green color) in cocrystal structure with the same protein. Cocrystal structure of **14** with monomeric L858R/T790M EGFR demonstrates that the CF_3 binds in the G loop hydrophobic pocket.

Table 2: Summary of Initial Aliphatic Linker Designs.

Compound ID	Structure	K_i^{est} (nM)	k_{obs}/I ($M^{-1}s^{-1}$)	H1975 IC_{50} (nM)	WT IC_{50} (μM)	WT/DM	Log D[a]	HLM Cl[b] (μL/min/g)	RRCK[c] (10^{-6} cm/sec)	GSH $T_{1/2}$ relative to canertinib[e]
13	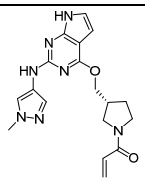	590	830 (at 1 μM)[e]	ND	ND	ND	2.1	56	16	ND
14	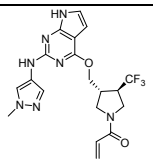	35	5,410 (at 1 μM)[e]	47	>5	>106	2.7	26	11	9
15	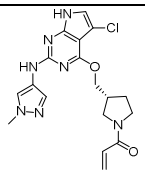	8	19,100 (at 0.1 μM)[e]	45	>3.3	>73	2.91	45	13	>19
16	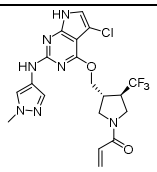	3	51,400 (at 0.05 μM)[e]	8	3.5	438	3.0	37	3	9

[a]log *D* was measured at *p*H 7.4. [b]Human liver microsomal intrinsic clearance. [c]Permeability measured with low-efflux MDCKII cell. [d]Chemical reactivity of warhead relative to canertinib (half-life in glutathione buffer at *p*H 7.4). [e]Inhibitor concentration at which the k_{obs}/I is calculated.

To help understand the binding mode and ligand conformation of **14**, its co-crystal structure was determined at 2.2 Å resolution (Figure 11). Although the crystal structure does not reflect the transition state conformation for the covalent bond formation between Cys797 and the warhead

acrylamide, it is evident that the conformation of the linker -OCH_2- is constrained in an orientation *syn* to the nitrogen of the pyrimidine. The pyrrolidine occupies the space extending from the sugar binding pocket to the triphosphate recognition site of the active site, and the substituents at the 3 and 4-positions of the pyrrolidine ring adopt a *trans* di-axial conformation. Ligand torsional profile analysis suggests that the minimum energy conformation of **14** in solution has the linker -OCH_2- co-planar with the core. In contrast, the bound conformation has the -OCH_2- rotated out of conjugation to the core, resulting in a strain energy penalty (~1.4 kcal/mol, calculated with Amber force field) which is compensated for by the binding energy gained from the strong interactions between the CF_3 and the protein.

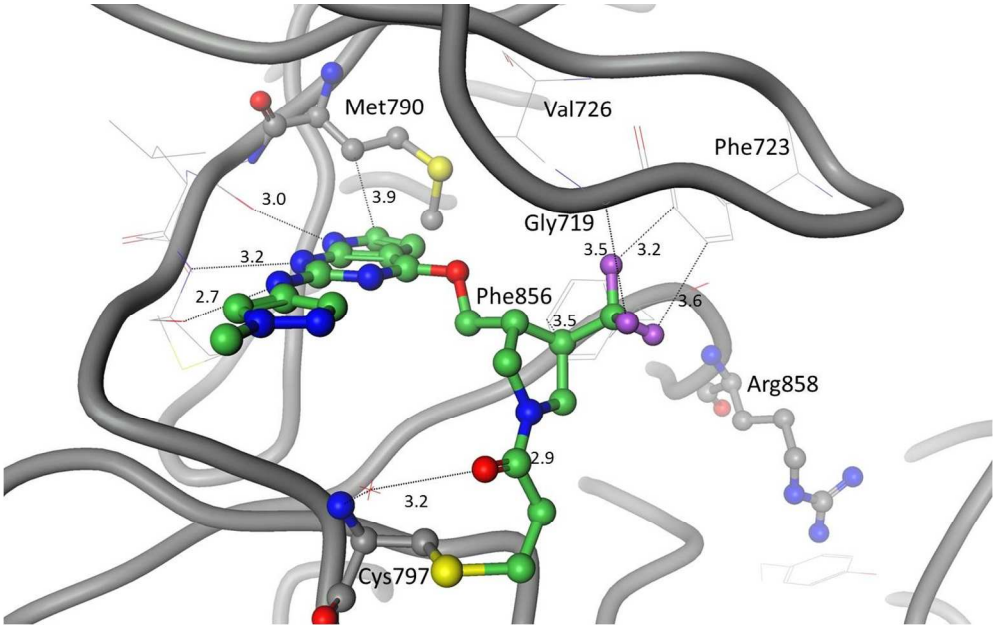

Figure 11. Crystal structure of **14** in complex with monomeric L858R/T790M EGFR (2.2 Å). The CF_3 group fills a small hydrophobic pocket affording a 17-fold increase in binding affinity. Note interaction between the CF3 group and Phe723 and Phe526.

5-Cl Pyrrolopyrimidine Scaffold Significantly Increases Intrinsic Binding Affinity.

The cocrystal structure of **14** also revealed an opportunity to increase binding affinity *via* targeting an unoccupied hydrophobic pocket near the gatekeeper residue. Placing a halogen at the 5-position of the pyrrolopyrimidine was predicted to fill this pocket. A Cl substitution demonstrated significant increases in both binding affinity *and* irreversible inactivation (Table 2**)**. Relative to **13** and **14**, introduction of 5-Cl to afford **15** and **16** yielded a 74- and 12-fold increase in K_i^{est} respectively. In addition to the enhanced binding affinity, a substantial increase in the inactivation rate was achieved, with k_{obs}/I values of 19,100 and 51,400 $M^{-1}s^{-1}$ respectively. Computational analysis of ligand conformational energy profile predicts that introduction of the halogen at the 5-position will further constrain the linker in an optimal conformation to position the warhead to react with Cys797 (ligand torsional strain energy analysis to support this hypothesis is described in supporting information section). This, together with additional hydrophobic interactions with the G loop, yielded consistently potent aliphatic linkers (see pairwise plot, Figure 12) and provided the opportunity to optimize the linker in the absence of electron withdrawing groups. The intrinsic reactivity of compound **15** was more than 19-fold lower than that of canertinib, indicating that high potency, high inactivation rate and low intrinsic reactivity could all be achieved within the aliphatic linker sub-series.

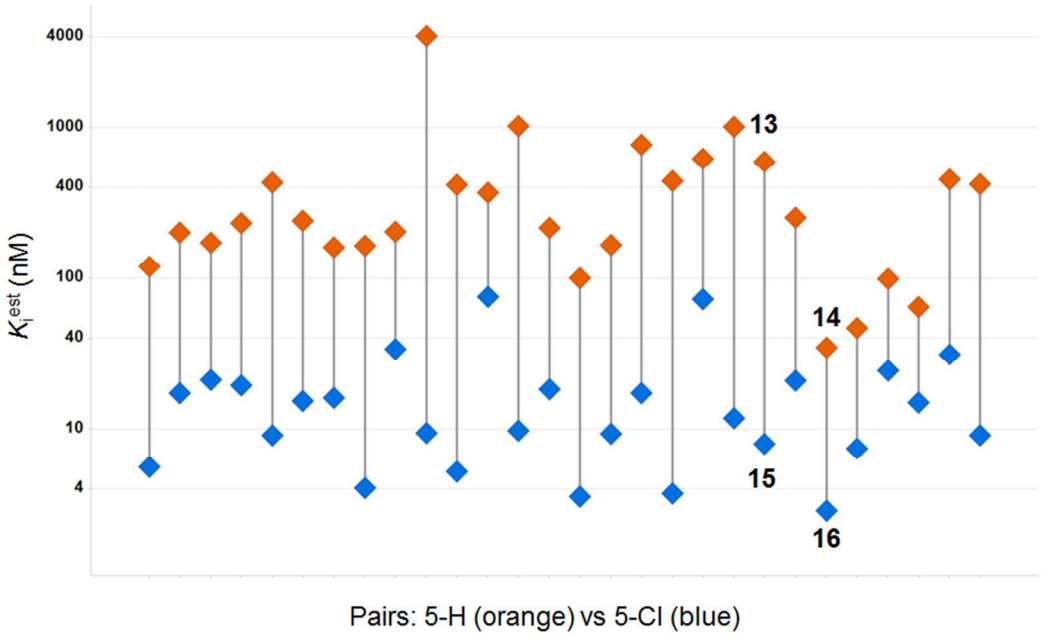

Figure 12. Pairwise comparison between 5-Cl and 5-H pyrrolopyrimidine analogs. Chlorine substitution of the 5-position of the PP core afforded a 47-fold average increase in binding affinity.

Lead Optimization.

Compound **15** had high permeability (RRCK 13 x10^{-6} cm/sec) with significant cellular activity (pEGFR H1975 IC_{50} 45 nM) and high selectivity over EGFR WT (>73x). However, the high metabolic clearance needed to be addressed in order to achieve a desirable human PK profile. The cocrystal structure of **14** reveals that the CF_3 binds very tightly in the G-loop hydrophobic pocket, with the CF_3 directly interacting with the Phe723 side chain phenyl ring (**Figure 10**). As half of the CF_3 moiety was exposed to solvent, it presented an opportunity to modulate metabolic stability by replacing the CF_3 with small polar groups. Based on the outcome from modeling studies and *in silico* ADME predictions -F, -OMe, -OH, -CH_2OH and -CH_2OMe replacements for –CF_3 were explored (Table 3).

Table 3: Summary of Lead Optimization.

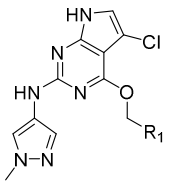

Compound ID	R^1	K_i^{est} (nM)	k_{obs}/I ($M^{-1}S^{-1}$)	H1975 IC_{50} (nM)	A549 IC_{50} (μM)	WT/DM	Log D[a]	LipE[b] (H1975 IC_{50})	HLM Cl[c] (μL/min/g)	RRCK[d] (10^{-6} cm/sec)	GSH $T_{1/2}$ relative to canertinib[e]
1	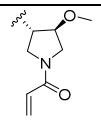	4	40,600 (at 0.05 μM)[f]	13	5.1	392	2.5	5.5	18	10	15
17	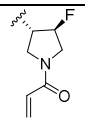	3	43,500 (at 0.05 μM)[f]	9	4.2	467	2.7	5.4	28	5	15
18	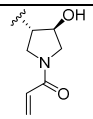	8	24,800 (at 0.1 μM)[f]	210	>10	>48	2.0	4.7	12	3	10
19	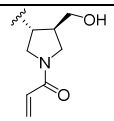	15	6,310 (at 1 μM)[f]	710	>10	>14	2.3	3.9	13	3	ND
20	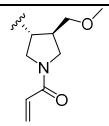	4	26,800 (at 0.05 μM)[f]	8	9.1	1140	2.9	5.3	23	16	>17
21	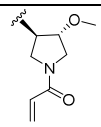	32	2,010 (at 1 μM)[f]	120	>10	>83	2.4	4.5	24	10	>17

[a]log *D* was measured at *p*H 7.4. LipE = - [log(H1975 cell IC_{50})] – log *D*. [c]Human liver microsomal intrinsic clearance. [d]Permeability measured with low-efflux MDCKII cell. [e]Chemical reactivity of warhead relative to canertinib (half-life in glutathione buffer at *p*H 7.4). [f]Inhibitor concentration at which the k_{obs}/I is calculated.

Pyrrolidine derivatives **1** (PF-06459988), **17**-**20** demonstrate potent affinity and high inactivation rates with an improvement in metabolic stability relative to compound **16**. In the cellular assay, **1**, **17** and **20** were highly potent against L858R/T790M DM and highly selective over WT. Compound **18** and **19**, substituted with an alcohol or hydroxymethyl at the 4-position of the pyrrolidine ring, exhibited low permeability and consequently reduced cellular potency. Compound **1** emerged as providing the best balance of overall properties including potency, WT selectivity, intrinsic chemical reactivity, ADME properties, and the highest LipE. Its enantiomer (**21)** exhibited a k_{obs}/I of 2,010 $M^{-1}s^{-1}$, indicating modest to no irreversible inhibition, and was less potent in both the enzyme assay (K_i^{est} = 32 nM) and the cellular assay (H1975 cell IC_{50} = 120 nM). This suggests the optimum alignment of the acrylamide warhead with Cys797 is critical for the observed high potency for **1**.

A 1.9 Å co-crystal structure of **1** in complex with EGFR L858R/T790M DM shows a great deal of similarity to that of **14** (Figure 13). The substituents at the 3- and 4-positions of the pyrrolidine ring adopt a trans-diaxial conformation, which places the polarized methyl of the methoxy group at the 4-position in van der Waals contact with the aromatic side chain of Phe856, which in turn interacts edge to face with the sidechain phenyl of Phe723. In addition, the Cl substituent at the 5-position of the PP core interacts with both the Phe856 side chain and the Met790 side chain through hydrophobic interactions. Ligand strain energy analysis using Bachmin V2.0[37] indicates that the bound conformation of compound **1** possess minimal strain energy (see SI for details), which is consistent with the very high binding affinity and cellular potency that it demonstrates against L858R/T790M mutant.

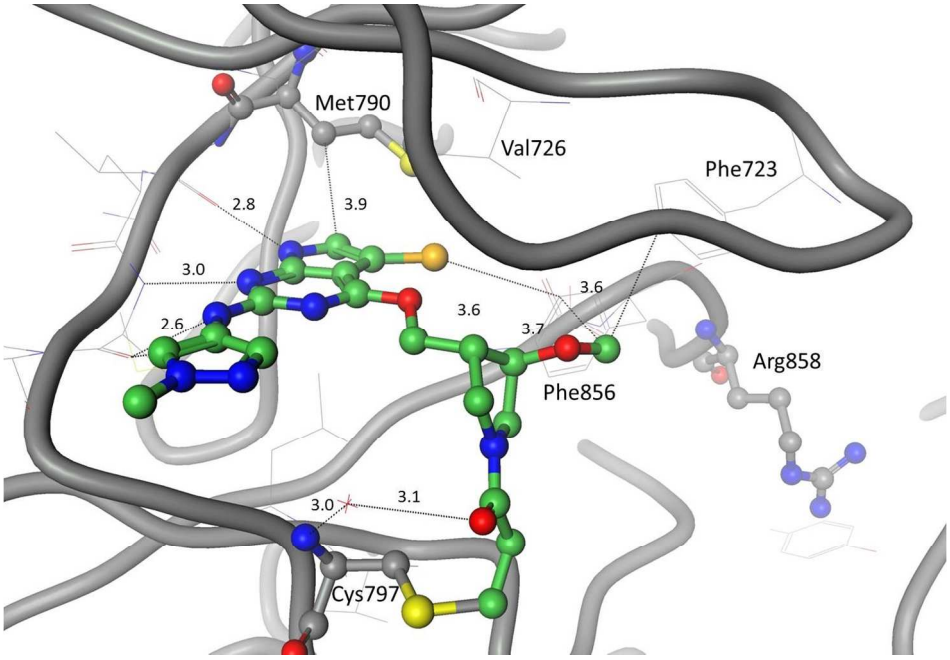

Figure 13. Crystal structure of **1** in complex with monomeric L858R/T790M EGFR (1.9 Å). The diaxial conformation of the pyrroldine places the OMe in van der Waal's contact with both the Phe856 of the DFG motif and the Phe723 of the G-loop.

Characterization of compound 1.

Since compound **1** emerged as a project lead by having the best overall balance of properties, it was characterized in detail in both biochemical and cellular assays (Table4, 5, SI-1, SI-2). Compound **1** is a potent and efficient inhibitor of EGFR L858R/T790M DM (K_i = 13 nM, k_{inact} = 0.02 s^{-1}, k_{inact}/K_i = 1,530,000 $M^{-1}s^{-1}$), and shows modest activity toward WT EGFR (K_i^{est} = 1,600 nM, k_{inact}/K_i^{est} = 4,520 $M^{-1}s^{-1}$, Table SI-1). Its cellular biochemical potency was characterized in NSCLC cell lines including H1975 (L858R/T790M), PC9-DRH (Del/T790M), H3255 (L858R), PC9 (Del), HCC827 (Del) and A549 (WT) (Table 4). rociletinib, osimertinib and erlotinib were also evaluated in the same NSCLC cell lines. Compound **1,** rociletinib and osimertinib all

demonstrate very high cellular potency against T790M-containing double mutant EGFRs. Rociletinib and osimertinib demonstrate good cellular potency against the oncogenic mutants L858R and Del. In comparison, **1** also demonstrates good cellular potency against L858R mutant, albeit moderate cellular potency against Del mutant in the PC9 cell line. Erlotinib demonstrates very high cellular potency against both oncogenic mutants and WT EGFR, but is inactive against T790M-containing double mutants. Compound **1** spares WT EGFR, hence demonstrates the highest selectivity between the least potent target and WT EGFR.

Table 4: Cellular Potency and Selectivity Profile of 1, Rociletinib, Osimertinib and Erlotinib

	L858R/ T790M	Del/ T790M	L858R	Del	Del	WT	WT/DM (L858R/ T790M)	WT/least potent target
Compound	H1975 IC_{50} (nM)	PC9-DRH IC_{50} (nM)	H3255 IC_{50} (nM)	PC9 IC_{50} (nM)	HCC827 IC_{50} (nM)	A549 IC_{50} (nM)	Ratio	Ratio
1	13	7	21	140	90	5,100	392	36
Rociletinib	16	9	46	79	65	1,600	100	20
Osimertinib	15	13	36	56	23	150	10	3
Erlotinib	9,000	9,700	10	11	8	11	0.0012	1

Proteome-Wide Selectivity.

Cysteine is the most intrinsically nucleophilic proteinaceous residue, and many protein classes rely on cysteine for function.[38] Irreversible EGFR inhibitors with high intrinsic reactivity for the warhead have the potential to cross-react, either specifically or nonspecifically, with other proteins, including those outside the kinome, which may lead to unanticipated toxicities. To compare the broad proteome reactivity between **1** (GSH reactivity ratio = 15) and canertinib (GSH reactivity ratio =1), clickable probes of these two compounds were designed to enable activity-based protein profiling by installing the alkyne at positions that would neither perturb the intrinsic reactivity of the Michael acceptors nor interfere with the binding to EGFR.

Physiochemical and biological properties for the probe for canertinib (**22**) and the probe for **1** (**23**), including cellular IC_{50} against wild type and double mutant EGFR, and K_{obs}/I and GSH reactivities, closely matched the properties for canertinib and **1**, respectively (Table 5).

Table 5. Comparison of Properties for 1 and canertinib with Their Corresponding Probes.

ID	Structure	Ki^{est} (nM)	K_{obs}/I $M^{-1}s^{-1}$	H1975 IC_{50} (nM)	WT IC_{50} (nM)	LogD[a]	RRCK[b] (10^{-6} cm/sec)	GSH $T_{1/2}$ relative to canertinib[c]
Canertinib	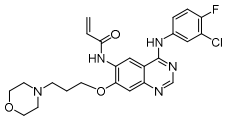	0.11	148,000 (at 0.01 μM)[d]	3	6	ND	ND	1
22	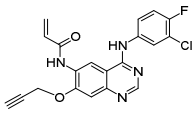	2	48,600 (at 0.05 μM)[d]	7	15	4.0	0.4	1.2
1	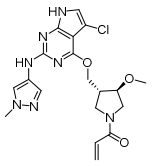	4	40,600 (at 0.05 μM)[d]	13	5,100	2.5	10	15
23	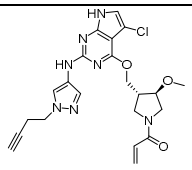	10	17,300 (at 0.1 μM)[d]	16	4,200	3.0	7	>17

[a]log *D* was measured at pH 7.4. [b]Permeability measured with low-efflux MDCKII cell. [c]Chemical reactivity of warhead with glutathione relative to canertinib at pH 7.4. [d]Inhibitor concentration at which the k_{obs}/I is calculated.

Initial experiments were performed in the EGFR L858R/T790M mutant H1975 lung cancer cell line. *In situ* reactivity of the two probes by gel-based analysis was derived from an H1975 in vitro experiment, where cells were treated with 1 μM of compound for 15 minutes to 24 hours before the H1975 cells were harvested (Figure 14). Fractionated cellular lysates were reacted with azide-rhodamine (N_3-Rh) under standard copper-catalyzed azide-alkyne cycloaddition (CuACC) conditions.[39] Covalently probe-modified proteins were revealed by their in-gel fluorescence. Both chemical probes displayed increasing amounts of proteome reactivity in the soluble (Figure 14, top) and particulate (Figure 14, bottom) proteomes as the length of probe incubation was increased. Compound **23** (probe to **1**) displayed a slower, gradual increase in reactivity compared to **22** (probe to canertinib). The covalently modified proteins included both overlapping and unique targets. The identification of the covalent targets will be revealed in a later manuscript. In agreement with their warhead intrinsic chemical reactivity, considerably more proteome reactivity was observed for **22** than for **23**. This was especially apparent at a 1 hour timepoint in H1975 cells (Figure SI-1A in SI) where a more than 50% reduction in total off-target labeling signal was observed (Figure SI-1B in SI). Similarly, more off-target labeling in H3255 cells was observed, where H3255 expresses only the L858R single mutant form of EGFR (Figure SI-1C in SI).

Thus, by minimizing the intrinsic chemical reactivity of the electrophilic warhead, **1** demonstrates significantly increased proteome wide selectivity over canertinib. This is likely one of the reasons that only minimal findings were observed from toxicity studies with **1**, with

duration up to one month in mice and dogs at in vivo exposures exceeding antitumor efficacy levels.

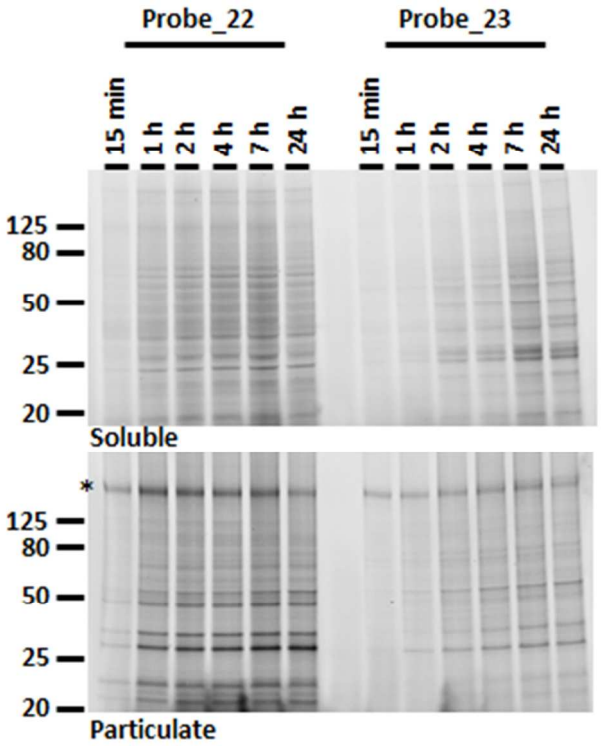

Figure 14. Time course in situ labeling profiles of 1 μM of **22** (probe to canertinib, left) and **23** (probe to **1**, right) in H1975 cells separated into soluble (top) and particulate (bottom) proteomes. H1975 cells were treated for 15 min to 24 h before being harvested. Lysates were analyzed by gel-based florescence and gels are shown in grayscale. A specific protein with the molecular weight matching that of EGFR is highlighted with a * in the particulate proteome.

The kinase selectivity of **1** was evaluated by multiple biochemical methodologies and the compound was judged to have moderate kinase selectivity (for details, see supporting information section). A variety of in vitro and in vivo safety studies with **1** were also carried out to understand the potential safety risks due to its moderate kinase selectivity. The potential risks did not translate under more physiologically-relevant conditions (i.e. functional in vitro assays, and at in vivo exposures exceeding antitumor efficacy levels).

When evaluated in PK/PD and TGI studies in mice implanted with tumor cell lines harboring T790M-containing double mutants L858R/T790M and Del/T790M, **1** demonstrated robust PK/PD correlation and tumor growth inhibition. A manuscript discussing the results from these in vivo studies including PK/PD and TGI studies will be disclosed in due course.

CHEMISTRY.

The synthesis of compounds **10-12** began with the incorporation of the trimethylsilylethoxymethyl or SEM-protecting group[40] to 2,4-dichloro-7H-pyrrolo[2,3-d]pyrimidine **24** using SEM-Cl and LiHMDS to give **25** (Scheme 1). The phenoxy linker in intermediate **26** was then introduced using *tert*-butyl(3-hydroxyphenyl)carbamate and potassium carbonate. Attachment of the key hinge binding heteroaromatic amino side chains was achieved using Buchwald-Hartwig aminations under microwave conditions to yield the amines **27-29**. Selective deprotection of the Boc group in compound **27** and **28** followed by acryloylation gave the acrylamides **30** and **31**. A two-step deprotection of the SEM protecting group was done using trifluoroacetic acid in the first step which led to partial cleavage of the SEM protecting group giving intermediates **32** and **33** containing an N-hydroxymethyl moiety. Although these intermediates were not isolated, they were observable by ^{1}HNMR and showed a characteristic peak at δ 5.38 (see Supplementary Information for the ^{1}HNMR of intermediate **32**).[40] The deprotection was completed by treating these intermediates with potassium carbonate to yield the final acrylamides **10** and **11**. Alternatively, acrylamide **12** was obtained by deprotection of the Boc group and partial deprotection of the SEM protecting group in compound **29** using TFA, acryloylation followed by final deprotection.

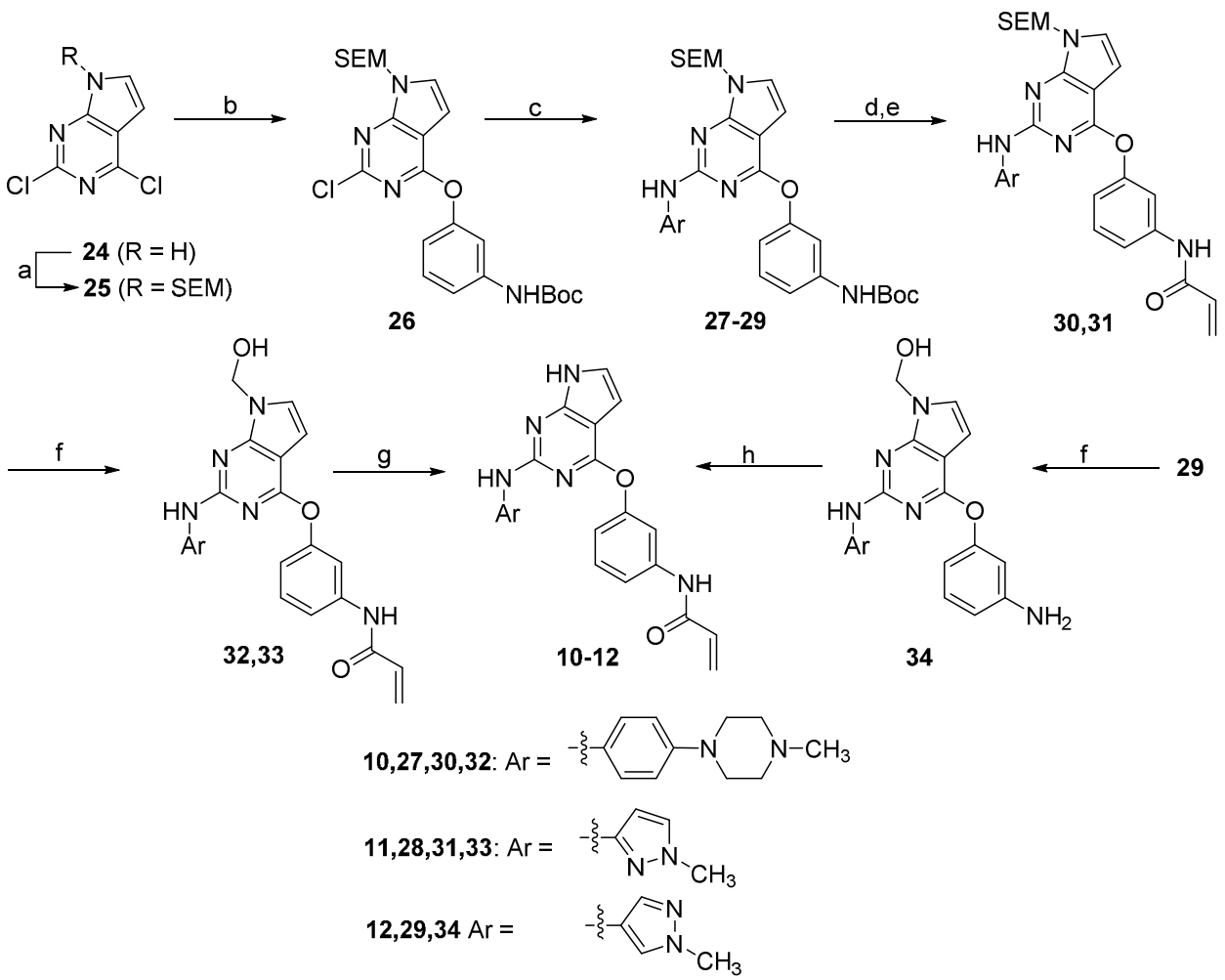

Scheme 1: a. $TMSCH_2CH_2OCH_2Cl$, LiHMDS, THF, 79%; b. *tert*-butyl(3-hydroxyphenyl)carbamate, K_2CO_3, MeCN, 90%; c. $ArNH_2$, $Pd_2(dba)_3$, Cs_2CO_3, Xantphos, 1,4-dioxane, μW, 43-87%; d. HCl, 1,4-dioxane; e. CH_2=CHCOCl, DCM or THF 65-70% (steps d and e); f. TFA, DCM; g. K_2CO_3, MeOH or EtOH, 46-77% (steps f and g); h. i) CH_2=CHCOCl, DCM, ii) K_2CO_3, EtOH, 47% (steps f and h).

Compounds **13** and **23** were synthesized in a similar fashion starting from pyrrolo[2,3-d]pyrimidine **25** and reacting it with the alcohols **35** and **36** under basic conditions (Scheme 2). The installation of the amino pyrazole was done using Buchwald-Hartwig amination conditions and this was followed by the aforementioned two-step deprotection protocol to remove the Boc- and SEM-protecting groups. Acryloylation of the corresponding pyrrolidines to the acrylamides **13** and **23** was carried out under carefully monitored conditions using DIPEA and acryloyl chloride to minimize bis-acryloylated side products.

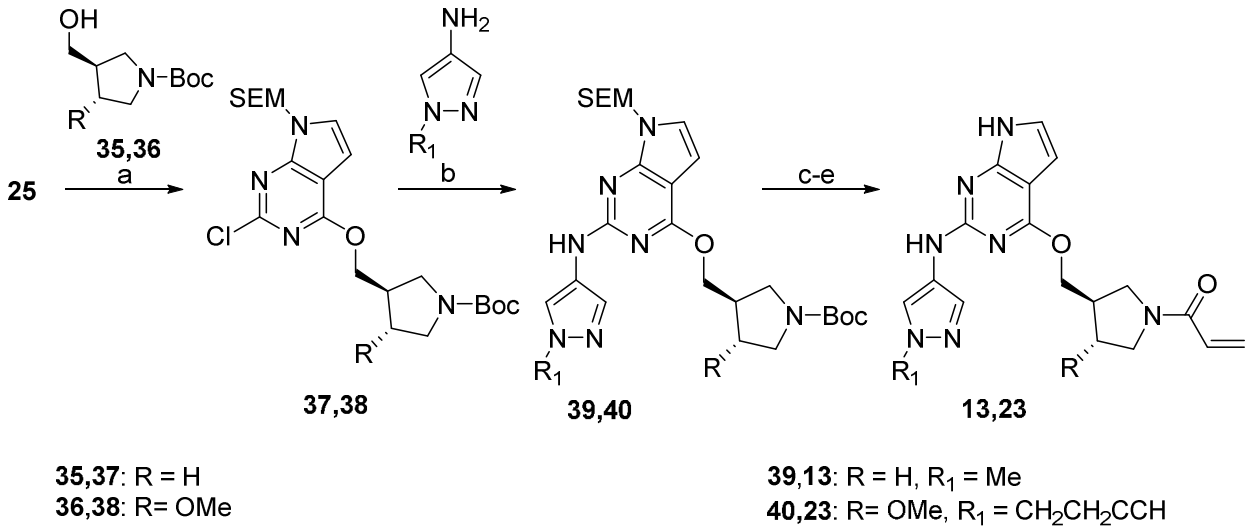

Scheme 2: a. KHMDS, 1,4-dioxane; b. 1-alkyl-1H-pyrazol-4-amine, $Pd_2(dba)_3$, Cs_2CO_3, Xantphos, 1,4-dioxane, µW; c. TFA, DCM; d. K_2CO_3, MeOH, H_2O or NH_4OH, 1,4-dioxane; e. CH_2=CHCOCl, DIPEA, DCM or CH_2=CHCOCl, THF, **13**: 0.9% over 5 steps; **23**: 11% over 5 steps.

Route optimization efforts were initiated to overcome the harsh conditions required for the Buchwald-Hartwig amination step and to avoid the need for the capricious *N*-SEM protecting group. To this end, a 196-well screen using two solvents; 1,4-dioxane and toluene, two bases; cesium carbonate and potassium *tert*-pentoxide and 48 catalyst-ligand combinations was utilized to review the amination of an unprotected model substrate, 4-(benzyloxy)-2-chloro-7H-pyrrolo[2,3-d]pyrimidine **41**, with 1-methyl-1H-pyrazol-4-amine (Scheme 3).

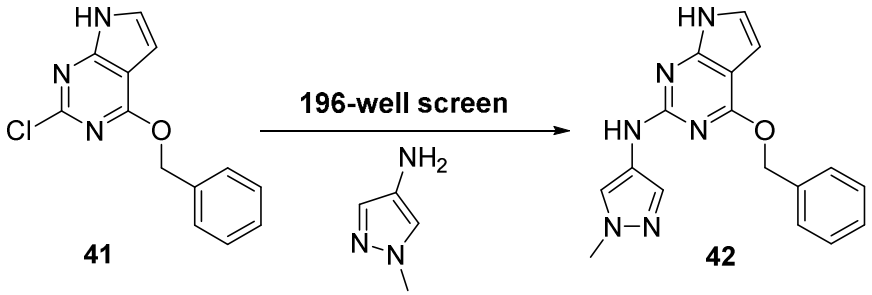

Scheme 3: 196-well amination screen.

This screening effort led to the finding that the Buchwald-Hartwig amination can indeed be carried out under milder conditions using an unprotected 2-chloro-pyrrolo[2,3-d]pyrimidine core. The optimized conditions for the amination were *tert*-BuXPhos palladacycle and potassium *tert*-pentoxide in 1,4-dioxane at 90 °C. Further refinement of the sequence led to the discovery of an efficient one-pot protocol (Scheme 4) wherein excess potassium *tert*-pentoxide (4 equivalents) was used as the base to append the alkoxy linker using an appropriate alcohol and 1,4-dioxane as solvent in the first step. After 30 minutes of aging, *tert*-BuXPhos palladacycle and the appropriate amine were added to the same pot and the reaction mixture was warmed to 90 °C to complete the incorporation of the heteroaromatic amino side chain. After purification, the Boc-protecting group was cleaved using trifluoroacetic acid to give **46**. Further optimization of the final acryloylation step indicated that Schotten-Baumann conditions using aqueous sodium bicarbonate and acryloyl chloride in ethyl acetate were most optimal for a robust acryloylation. The synthesis of acrylamide **1** (Scheme 4) illustrates the effectiveness of this atom-economic sequence. This sequence was also used to synthesize the acrylamides **14**-**21** using appropriate alcohols to introduce the relevant alkoxy linkers (see Supporting Information for details).

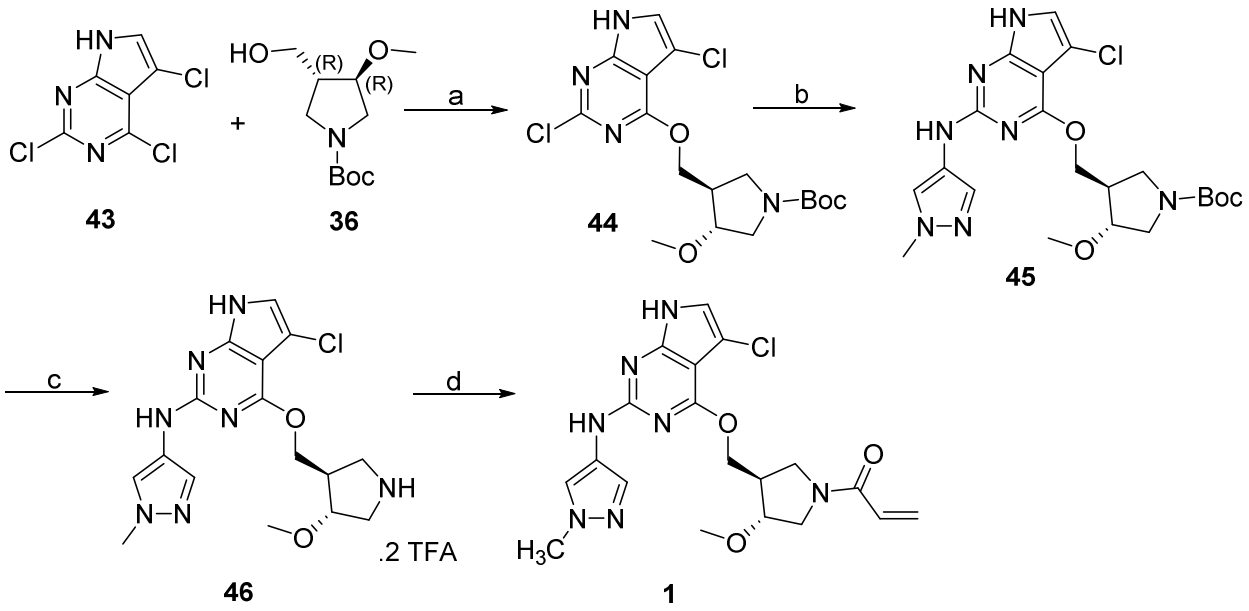

Scheme 4. a. Potassium *tert*-pentoxide, 1,4-dioxane b. 1-methyl-1H-pyrazol-4-amine, *tert*-BuXPhos palladacycle, 79% over two steps; c. TFA, DCM, 99%; d. CH_2=CHCOCl, aq. $NaHCO_3$, EtOAc, 77%.

The synthesis of the chiral alcohol **36** was achieved as outlined in Scheme 5. A [3+2]-cycloaddition reaction of methyl (*E*)-3-methoxyacrylate (**47**) with an azomethine ylide generated *in-situ* from *N*-benzyl-1-methoxy-*N*-((trimethylsilyl)methyl)methanamine (**48**) provided the racemic pyrrolidine ester **49**. Chiral separation of this racemic ester using chiral supercritical fluid chromatography (SFC) yielded the requisite enantiomer **50**. The benzyl protecting group in **50** was then removed under hydrogenolysis conditions and replaced with a Boc protecting group using Boc_2O. The final step involved the reduction of the ester using lithium borohydride which yielded (3*R*,4*R*)-**36**.

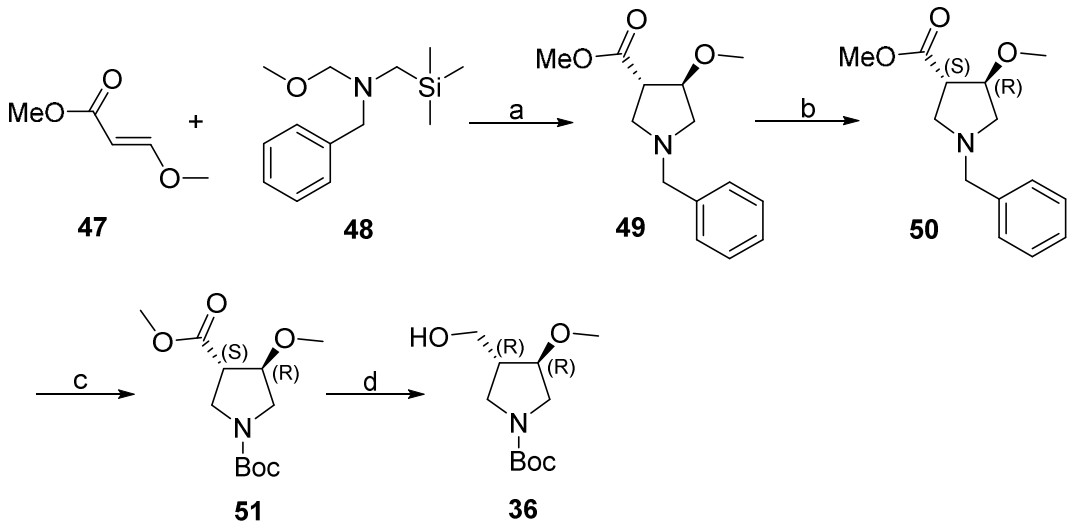

Scheme 5. a. **48**, TFA, 73%; b. Chiral-SFC (Chiralpak AD-H) 32%; c. i. H_2 (1 atm), 10% $Pd(OH)_2$ (6%), EtOH ii. Boc_2O, 98%; d. $LiBH_4$, THF, 92%.

CONCLUSION.

Compound **1** has been discovered as a potent irreversible inhibitor of T790M mutant EGFR, having excellent selectivity against EGFR WT whilst possessing a minimally reactive electrophile that reduces the propensity of off-target labelling. Critical to the success of the program was the development of an assay capable of separating out the affinity and reactivity components that contribute to the overall potency of each inhibitor. This enables affinity driven SAR. Proteomic evaluation of **1** in H1975 cells confirmed a reduction of off-target labelling relative to canertinib. Follow-up efforts to optimize kinome selectivity and potency against the oncogenic EGFR Del will be published in due course.

EXPERIMENTAL SECTION.

General. Starting materials and other reagents were purchased from commercial suppliers and were used without further purification unless otherwise indicated. All reactions were performed under a positive pressure of nitrogen, argon, or with a drying tube, at ambient temperature (unless otherwise stated), in anhydrous solvents, unless otherwise indicated. Analytical thin-layer chromatography was performed on glass-backed Silica Gel 60_F 254 plates (Analtech (0.25mm)) and eluted with the appropriate solvent ratios (v/v).

The reactions were assayed by high performance liquid chromatography (HPLC) or thin-layer chromatography (TLC) and terminated as judged by the consumption of starting material. The TLC plates were visualized by phosphomolybdic acid stain, or iodine stain. Microwave assisted reactions were run in a Biotage Initiator. ^{1}H NMR spectra were recorded on a Bruker instrument operating at 400 MHz unless otherwise indicated. ^{1}H NMR spectra are obtained as DMSO-d_6 or $CDCl_3$ solutions as indicated (reported in ppm), using chloroform as the reference standard (7.25 ppm) or DMSO-d_6 (2.50 ppm). Other NMR solvents were used as needed. When peak multiplicities are reported, the following abbreviations are used: s = singlet, d = doublet, t = triplet, m = multiplet, br =broadened, dd = doublet of doublets, dt = doublet of triplets. Coupling constants, when given, are reported in hertz. The mass spectra were obtained using liquid chromatography mass spectrometry (LC-MS) on an Agilent instrument using atmospheric pressure chemical ionization (APCI) or electrospray ionization (ESI). High resolution mass measurements were carried out on an Agilent TOF 6200 series with ESI. All test compounds showed > 95% purity as determined by combustion analysis or by high-performance liquid chromatography (HPLC). HPLC conditions were as follows: XBridge C18 column @ 80 °C, 4.6 mm x 150 mm, 5 μm, 5%-95% MeOH/H_2O buffered with 0.2% formic acid/0.4% ammonium

formate, 3 min run, flow rate 1.2 mL/min, UV detection (λ = 254, 224 nm). Combustion analyses were performed by Atlantic Microlab, Inc. (Norcross, Georgia).

2,4-Dichloro-7-{[2-(trimethylsilyl)ethoxy]methyl}-7H-pyrrolo[2,3-d]pyrimidine (**25**). In a 1000 mL flask, LiHMDS (140 mL, 140 mmol) was diluted in dry THF (100 mL) and cooled to -78 ºC. 2,4-Dichloro-7H-pyrrolo[2,3-d]pyrimidine (25.0 g, 133 mmol) was suspended in THF (200 mL) using gentle warming and sonication. This suspension was added dropwise to the LiHMDS solution over 30 min. Additional THF (50 mL) was used to dissolve any residue from the flask and this suspension was also added dropwise to the LiHMDS solution. After complete addition, the mixture was allowed to stir at -78 ºC for 30 min. SEM-Cl (25 mL, 140 mmol) was added dropwise to the mixture and stirring was continued at -78 ºC for 30 min. The ice bath was allowed to slowly warm to room temperature overnight. The reaction was quenched by the addition of cold water (150 mL). EtOAc (200 mL) was added and the layers separated. The resulting aqueous layer was extracted with EtOAc (two x 200 mL). The combined organics were washed with brine (2X) and dried over $MgSO_4$, filtered and concentrated. The orange oil was purified via gravity "plug" chromatography eluting with 80 % heptanes / 20 % DCM to afford the title compound (33.4 g, 79% yield) as an orange oil which solidified upon standing: LC-MS (APCI) *m/z* for $C_{12}H_{17}Cl_2N_3OSi$ 318.00 / 320.05 $(M+H)^+$ for Cl isotopes; ^1H NMR (400 MHz, $CDCl_3$) δ 7.38 (d, *J* = 3.78 Hz, 1 H), 6.67 (d, *J* = 3.53 Hz, 5 H), 5.61 (s, 2 H), 3.50 - 3.59 (m, 2 H), 0.85 - 0.99 (m, 2 H), -0.03 (s, 9 H).

***Tert*-Butyl{3-[(2-chloro-7-{[2-(trimethylsilyl)ethoxy]methyl}-7H-pyrrolo[2,3-d]pyrimidin-4-yl)oxy]phenyl}carbamate (26)**. To a solution of **25** (1470 mg, 4.62 mmol) in acetonitrile (10 mL) was added *tert*-butyl (3-hydroxyphenyl)carbamate (966 mg, 4.62 mmol) and K_2CO_3 (1280 mg, 9.24 mmol) and the mixture heated at 80 °C overnight. The reaction was cooled to room

temperature, EtOAc (20 mL) was added, the mixture was washed with water (50 mL), the aqueous layer extracted with EtOAc (three x 20 mL), dried with $MgSO_4$, filtered and concentrated to give a light oil. Upon standing, the light oil solidified to give the title compound (2.05 g, 90 % yield) as a tan solid: LC-MS (ESI) *m/z* for $C_{23}H_{31}ClN_4O_4Si$ 491.20 $(M+H)^+$; ^1H NMR (400 MHz, DMSO-d_6) δ 9.38 - 9.83 (m, 1 H) 7.73 (d, *J* = 3.78 Hz, 1 H) 7.41 - 7.46 (m, 2 H) 7.51 (s, 1 H) 6.97 (dt, *J* = 5.98, 2.68 Hz, 1 H) 6.58 (d, *J* = 3.78 Hz, 1 H) 5.64 (s, 2 H) 3.54 - 3.67 (m, 2 H) 1.54 (s, 9 H) 0.91 - 0.96 (m, 2 H) 0.00 (s, 9 H).

General Procedure for the Synthesis of Anilines 27-29. To a solution of **26** (0.61 mmol) in 1,4-dioxane (4 mL) in a microwave vial was added the amine (0.61 mmol) followed by Cs_2CO_3 (0.915 mmol), $Pd_2(dba)_3$ (0.009 mmol) and Xantphos (0.009 mmol) and the mixture was heated in the microwave at 140 °C for 45 min. The reaction was cooled to room temperature, brine (20 mL) was added and the mixture was extracted with EtOAc (3 X 10 mL). The combined extracts were dried over $MgSO_4$, filtered and concentrated to give the anilines.

***Tert*-butyl-(3-((2-((4-(4-methylpiperazin-1-yl)phenyl)amino)-7-((2-(trimethylsilyl)ethoxy)methyl)-7H-pyrrolo[2,3-d]pyrimidin-4-yl)oxy)phenyl)carbamate** (**27**): Purified over silica gel with gradients from 100% heptane to 90% ethyl acetate-10% ammonia in methanol (7N) to yield the title product (1.56 g, 81% yield): LC-MS (APCI) *m/z* 646.3 $(M+H)^+$; ^1H NMR (400 MHz, DMSO-d_6) δ 9.60 (s, 1 H) 9.08 (s, 1 H) 7.59 (d, *J* = 8.31 Hz, 2 H) 7.46 - 7.53 (m, 2 H) 7.40 - 7.46 (m, 1 H) 7.29 (d, *J* = 3.78 Hz, 1 H) 6.95 (d, *J* = 8.06 Hz, 1 H) 6.81 (d, *J* = 8.81 Hz, 2 H) 6.40 (d, *J* = 3.53 Hz, 1 H) 5.57 (s, 2 H) 3.64 (t, *J* = 8.06 Hz, 2 H) 3.03 - 3.18 (m, 4 H) 2.48 - 2.56 (m, 4 H) 2.31 (s, 3 H) 1.55 (s, 9 H) 0.95 (t, *J* = 8.06 Hz, 2 H) 0.00 (s, 10 H).

***Tert*-butyl-(3-((2-((1-methyl-1H-pyrazol-3-yl)amino)-7-((2-(trimethylsilyl)ethoxy)methyl)-7H-pyrrolo[2,3-d]pyrimidin-4-yl)oxy)phenyl)carbamate** (**28**): Purified over silica gel with gradients from 0% to 10% methanol in dichloromethane to yield the title product (1446 mg, 87% yield); LC-MS (APCI) *m/z* 552.25 $(M+H)^+$; ^{1}H NMR (400 MHz, DMSO-d_6) δ 9.49 (s, 1 H) 9.29 (s, 1 H)7.28 - 7.46 (m, 4 H) 7.19 (d, *J* = 3.53 Hz, 1 H) 6.87 (d, *J* = 7.55 Hz, 1 H) 6.34 (br. s., 1 H) 6.20 (d, *J* = 3.53 Hz, 1 H) 5.47 (s, 2 H) 3.67 (s, 3 H) 3.50 - 3.57 (m, 2 H) 1.46 (s, 9 H) 0.77 - 0.89 (m, 2 H) -0.10 (s, 9 H).).

***Tert*-butyl-(3-((2-((1-methyl-1H-pyrazol-4-yl)amino)-7-((2-(trimethylsilyl)ethoxy)methyl)-7H-pyrrolo[2,3-d]pyrimidin-4-yl)oxy)phenyl)carbamate** (**29**): Purified over silica gel with gradients from 0% to 10% ethanol in 50% heptane:50% ethyl acetate to yield the title product (175 mg, 43% yield): LC-MS (APCI) *m/z* 552.20 $(M+H)^+$; ^{1}H NMR (400MHz, DMSO-d_6) δ 9.69 - 9.35 (m, 1H), 9.23 - 9.08 (m, 1H), 7.61 - 7.29 (m, 4H), 7.23 - 7.12 (m, 1H), 6.94 - 6.77 (m, 1H), 6.51 - 6.33 (m, 1H), 5.70 - 5.23 (m, 2H), 3.77 - 3.60 (m, 2H), 3.59 - 3.48 (m, 3H), 1.45 (s, 9H), 0.85 (s, 2H), -0.09 (s, 9H).

General Procedure for the Synthesis of acrylamides 30, 31

Step 1: To a solution of the pyrrolopyrimidines **27** or **28** (1 equivalent) in DCM (5mL) was added 4M HCl in dioxane (5 equivalents) and the reaction mixture was stirred at room temperature for 1 h. Evaporation of the solvent provided an intermediate which was taken on to the next step without further purification.

Step 2: To a solution of crude anilines (1 equivalent) in THF or DCM was added dropwise of prop-2-enoyl chloride (1 equivalent), and the mixture was stirred at room temperature for 0.25 to

1 h. Saturated aqueous $NaHCO_3$ (10 mL) was added and the product was extracted using EtOAc (3 X 10 mL), dried with $MgSO_4$, filtered, concentrated.

***N*-(3-((2-((4-(4-methylpiperazin-1-yl)phenyl)amino)-7-((2-(trimethylsilyl)ethoxy)methyl)-7H-pyrrolo[2,3-d]pyrimidin-4-yl)oxy)phenyl)acrylamide** (**30**): **P**urified over silica gel with a gradient of 0% to 10% methanol in ethyl acetate to yield the title product (288 mg, 76% yield, 2 steps): LC-MS (APCI) *m/z* 600.20 $(M+H)^+$; ^{1}H NMR (400 MHz, MeOH- d_4) δ 7.66 - 7.76 (m, 2 H) 7.58 (d, J=9.06 Hz, 2 H) 7.50 (t, J=8.18 Hz, 1 H) 7.14 (d, J=3.78 Hz, 1 H) 7.05 -7.11 (m, 1 H) 6.91 (d, J=9.06 Hz, 2 H) 6.40 - 6.57 (m, 3 H) 5.86 (dd, J=9.57, 2.27 Hz, 1 H) 5.62 (s, 2 H) 3.62 - 3.76 (m, 2 H) 3.13 - 3.28 (m, 4 H) 2.68 - 2.85 (m, 4 H) 2.47 (s, 3 H) 0.92 - 1.07 (m, 2 H) 0.00 (s, 9 H).

***N*-(3-((2-((1-Methyl-1H-pyrazol-3-yl)amino)-7-((2-(trimethylsilyl)ethoxy)methyl)-7H-pyrrolo[2,3-d]pyrimidin-4-yl)oxy)phenyl)acrylamide** (**31**): **P**urified over silica gel with a gradient of 0% to 10% methanol in dichloromethane to yield the title product (468 mg, 65% yield, 2 steps): LC-MS (APCI) *m/z* 506.20 $(M+H)^+$; ^{1}H NMR (400 MHz, DMSO- d_6) δ 10.27 (s, 1 H) 9.32 (s, 1 H) 7.63 - 7.67 (m, 1 H) 7.56 (d, *J* = 7.81 Hz, 1 H) 7.41 (t, *J* = 8.06 Hz, 1 H) 7.36 (s, 1 H) 7.21 (d, *J* = 3.53 Hz, 1 H) 7.00 (dd, *J* = 8.06, 2.27 Hz, 1 H) 6.38 - 6.48 (m, 1 H) 6.33 (br. s., 1 H) 6.28 (d, *J* = 2.01 Hz, 1 H) 6.21 - 6.26 (m, 1 H) 5.70 - 5.89 (m, 1 H) 5.48 (s, 2 H) 3.67 (s, 3 H) 3.54 (t, *J* = 8.06 Hz, 2 H) 0.85 (t, *J* = 8.06 Hz, 2 H) -0.09 (s, 9 H).

General procedure for the synthesis of acrylamides 10 and 11

Step 1: To a solution of the SEM-protected pyrrolopyrimidine in DCM (5 mL) was added TFA (3 mL) and the reaction mixture was stirred at room temperature for 4 h. Evaporation of solvent

provided the *N*-hydroxymethyl intermediate which was taken to the next step without further purification.

Step 2: To a solution of an *N*-hydroxymethyl intermediate in MeOH or EtOH (10 mL) was added K_2CO_3 and the reaction mixture was stirred at room temperature for 2 h. Water was added and the product was either extracted using EtOAc (3 X 20 mL), dried with $MgSO_4$, filtered, concentrated or precipitated out of solution, filtered and dried.

***N*-(3-((2-((4-(4-Methylpiperazin-1-yl)phenyl)amino)-7H-pyrrolo[2,3-d]pyrimidin-4-yl)oxy)phenyl)acrylamide (10)**: (174 mg, 77% yield): LC-MS (APCI) *m/z* 470.1 $(M+H)^+$; ^{1}H NMR (400 MHz, DMSO-d_6) δ 11.45 (br. s., 1 H) 10.28 (s, 1 H) 8.80 (s, 1 H) 7.56 - 7.67 (m, 2 H) 7.35 - 7.49 (m, 3 H) 7.03 (d, *J* = 3.53 Hz, 1 H) 6.94 - 7.00 (m, 1 H) 6.70 (d, *J* = 8.81 Hz, 2 H) 6.37 - 6.49 (m, 1 H) 6.18 - 6.32 (m, 2 H) 5.71 - 5.82 (m, 1 H) 2.91 - 3.05 (m, 4 H) 2.37 - 2.46 (m, 5 H) 2.21 (s, 3 H).

***N*-(3-((2-((1-Methyl-1H-pyrazol-3-yl)amino)-7H-pyrrolo[2,3-d]pyrimidin-4-yl)oxy)phenyl)acrylamide** (**11**): Purified over silica gel with a gradient of 0% to 20% ethanol in ethyl acetate to yield the title product (245 mg, 46% yield): LC-MS (APCI) *m/z* 376.15 $(M+H)^+$; ^{1}H NMR (400 MHz, DMSO-d_6) δ 11.48 (br. s., 1 H) 10.27 (s, 1 H) 9.13 (br. s., 1 H) 7.61 - 7.67 (m, 1 H) 7.57 (d, *J* = 8.06 Hz, 1 H) 7.41 (t, *J* = 8.18 Hz, 1 H) 7.30 (d, *J* = 2.01 Hz, 1 H) 7.05 (d, *J* = 3.53 Hz, 1 H) 6.99 (dd, *J* = 8.06, 1.76 Hz, 1 H) 6.36 - 6.48 (m, 1 H) 6.22 - 6.31 (m, 1 H) 6.10 - 6.21 (m, 2 H) 5.65 - 5.85 (m, 1 H) 3.66 (s, 3 H).

***N*-(3-((2-((1-Methyl-1H-pyrazol-4-yl)amino)-7H-pyrrolo[2,3-d]pyrimidin-4-yl)oxy)phenyl)acrylamide** (**12**). Step 1: To a solution of the SEM-protected pyrrolopyrimidine **29** in DCM (5 mL) was added TFA (3 mL) and the reaction mixture was stirred at room

temperature for 4 h. Evaporation of solvent provided the *N*-hydroxymethyl intermediate **34** which was taken on to the next step without further purification.

To a solution of aniline **34** (0.2 mmol) in DCM (4 mL) was added prop-2-enoyl chloride (0.2 mmol) and stirred at room temperature for 15 minutes. Ethanol (10 mL) was added to the reaction mixture followed by potassium carbonate (279 mg) and the mixture was stirred for 3 hours. The reaction mixture was then filtered, the filtrate was concentrated and the resultant residue was purified over silica gel with gradients from 0% to 20% ethanol in 50% heptane:50% ethyl acetate to yield the title product (36 mg, 47% yield); LC-MS (APCI) *m/z* 376.05 $(M+H)^+$; ^{1}H NMR (400 MHz, DMSO-d_6) δ 11.42 (br. s., 1 H) 10.33 (s, 1 H) 8.94 (s, 1 H) 7.58 - 7.73 (m, 2 H) 7.47 (t, *J* = 8.06 Hz, 1 H) 7.25 (br. s., 1 H) 6.93 - 7.11 (m, 2 H) 6.37 - 6.55 (m, 1 H) 6.28 (t, *J* = 16.24 Hz, 2 H) 5.77 (d, *J* = 10.07 Hz, 1 H) 3.62 (br. s., 3 H)

General Procedure for the Synthesis of 37, **38**: Potassium hexamethyldisilazide (1.5 mmol) was added to a mixture of **25** (1 mmol) and either alcohol **35** or **36** (1 mmol) in 1,4-dioxane (4 mL). The reaction mixture was stirred at room temperature for 2-16 h. LCMS showed the reaction was almost complete and the alkoxy ether products **37** and **38** obtained in this manner were taken on to the next step with no further purification.

General Procedure for the Synthesis of Amines 39, **40**: To a solution of **37** or **38** (1 mmol) in 1,4-dioxane or toluene and 2 drops of NMP in a microwave vial was added the appropriate amine (1.2 mmol) followed by Cs_2CO_3 (1.0-1.5 mmol), $Pd_2(dba)_3$ (0.05-0.1 mmol) and Xantphos (0.05-0.1 mmol) and the mixture was heated in the microwave at 140 °C for 45 min. The reaction was cooled to room temperature, brine (20 mL) was added and the mixture was extracted with EtOAc (3 X 10 mL). The combined extracts were dried over $MgSO_4$, filtered and

concentrated to give the amines **39** and **40** which were taken on to the next step with no further purification.

Synthesis of Acrylamides 13, 23

i. Two-step General Procedure for Global Deprotection of 39, 40

Step 1: To a solution of the SEM-protected pyrrolopyrimidine in DCM (5-10 mL) was added TFA (3 mL) and the reaction mixture was stirred at room temperature for 1-4 h. Evaporation of solvent provided the *N*-hydroxymethyl intermediates which were taken on to the next step with no further purification.

Step 2: To a solution of an *N*-hydroxymethyl intermediate in MeOH (10 mL) and water (2 mL) was added K_2CO_3. The reaction mixture was then stirred at room temperature for 2 h. Water was added and the product was extracted using EtOAc (3 X 20 mL), dried with $MgSO_4$, filtered and concentrated to a give the pyrrolidines that were taken to the next step with no further purification. Alternatively, in the case of the *N*-hydroxymethyl intermediate generated from **40**, ammonium hydroxide (4 mL) in 1,4-dioxane (8 mL) was utilized, the reaction mixture was stirred for 16 h and the product was then taken to the next step with no further purification.

ii. General procedure for Acrolylation

To a solution of crude pyrrolidine (1 equiv) in THF (10 mL) was added dropwise a solution of prop-2-enoyl chloride (1 equiv) in THF (1 mL). After addition, the mixture was stirred at room temperature for 1 h and then concentrated. The residue was purified by preparative HPLC to afford the acrylamides **13** and **23**.

(*R*)-1-(3-(((2-((1-Methyl-1H-pyrazol-4-yl)amino)-7H-pyrrolo[2,3-d]pyrimidin-4-yl)oxy)methyl)pyrrolidin-1-yl)prop-2-en-1-one (13): Purified by preparative HPLC by Phenomenex Gemini C18 4.6x100mm, 5 um column with H_2O (10% ammonia acetate)/CH_3CN @ 2.5 mL/min to give title compound (3.74 mg, 0.9% yield over 5 steps): LC-MS (APCI) *m/z* 368.20 $(M+H)^+$; ^1H NMR (700 MHz, DMSO-d_6) δ 8.86 (br. s., 1 H) 7.86-7.88 (m, 1 H) 7.50 (br. s., 1 H) 6.91(br. s, 1 H) 6.81 - 6.87 (m, 1 H) 6.60 - 6.62(m, 1H) 6.08 - 6.24 (m, 2 H) 6.02 (d, *J*=15.49 Hz, 1 H) 5.71 (d, *J*=10.33 Hz, 1 H) 5.50-5.51 (m, 1 H) 5.28(br. s, 1 H) 3.79 (s, 3 H) 3.28 - 3.38 (m, 1 H) 1.95 -2.17 (m, 2 H) 1.51-1.52 (m, 1 H).

1-((3*R*,4*R*)-3-(((2-((1-(But-3-yn-1-yl)-1H-pyrazol-4-yl)amino)-5-chloro-7H-pyrrolo[2,3-d]pyrimidin-4-yl)oxy)methyl)-4-methoxypyrrolidin-1-yl)prop-2-en-1-one (23): Purified via Prep-HPLC to give title compound (67 mg, 11% over 5 steps): LC-MS *m/z* 469.9 $(M+H)^+$; ^1H NMR (400 MHz, $CDCl_3$) δ 8.75 - 8.55 (d, 1H), 7.88 (s, 1H), 7.77 (s, 1H), 7.59 (s, 1H), 6.72 - 6.69 (d, 1H), 6.60 - 6.57 (d, 1H), 6.45 - 6.41 (m, 2H), 5.72 - 5.68 (m, 1H), 4.47 - 4.35 (t, 2H), 4.28 - 4.20 (m, 2H), 4.10 - 3.72 (m, 3H), 3.73 - 3.60 (m, 2H), 3.40 (s, 3H), 2.90 - 2.70 (m, 3H), 2.05 - 2.01 (m, 1H);

(3*R*,4*R*)-3-[5-Chloro-2-(1-methyl-1H-pyrazol-4-ylamino)-7H-pyrrolo[2,3-d]pyrimidin-4-yloxymethyl]-4-methoxy-pyrrolidine-1-carboxylic acid *tert*-butyl ester (45). To a solution 2,4,5-trichloro-7H-pyrrolo[2,3-d]pyrimidine (**43**) (9.28 g, 41.7 mmol) and (3*R*,4*R*)-3-hydroxymethyl-4-methoxy-pyrrolidine-1-carboxylic acid *tert*-butyl ester (**36**) (9.65 g, 41.7 mmol) in 1,4-dioxane (100 mL) was added potassium *tert*-pentoxide (25 % w/w in toluene, 80 mL, 167 mmol). The resulting reaction solution was stirred at ambient temperature for 30 min. LCMS showed a quantitative formation of (3*R*,4*R*)-3-(2,5-dichloro-7H-pyrrolo[2,3-d]pyrimidin-4-yloxymethyl)-4-methoxy-pyrrolidine-1-carboxylic acid tert-butyl ester (**44**). To the resulting

reaction solution was added 1-methyl-1H-pyrazol-4-ylamine (4.86 g, 50.1 mmol) and *t*-BuXPhos palladacycle (1.1 g, 1.67 mmol). The reaction mixture was stirred and heated at 90 °C in an oil bath for 1 h. The reaction mixture was filtered through Celite® and the filtrate was evaporated to remove the volatiles to give a dark gum that was dissolved in ethyl acetate (300 mL) and filtered through a silica gel plug. The filtrate was evaporated and the residue was purified via flash chromatography eluting with a gradient of 0 % – 100 % EtOAc in heptanes to give the title compound (12.4 g, 62% yield): LC-MS (APCI) *m/z* 378.2 $(M+H)^+$ for product minus Boc group with Cl isotope pattern; ^{1}H NMR (400 MHz, DMSO-d_6) δ 11.51 (br. s., 1 H) 9.07 (s, 1 H) 7.86 (s, 1 H) 7.52 (s, 1 H) 7.06 (d, *J* = 2.20 Hz, 1 H) 4.31 - 4.54 (m, 2 H) 3.92 (br. s., 1 H) 3.80 (s, 3 H) 3.55 - 3.68 (m, 1 H) 3.44 - 3.55 (m, 1 H) 3.30 (two singlets, OMe rotamers, 3 H) 2.72 (br. s., 1 H) 1.39 (br. s., 9 H).

[5-Chloro-4-((3*R*,4*R*)-4-methoxy-pyrrolidin-3-ylmethoxy)-7H-pyrrolo[2,3-d]pyrimidin-2-yl]-(1-methyl-1H-pyrazol-4-yl)-amine trifluoroacetate (46). To a solution of **45** (12.40 g, 26 mmol) in DCM (60 mL) at 0 °C was added TFA (10.1 mL, 208 mmol) and the resulting solution was stirred at ambient temperature for 2.5 h. The volatiles were removed and ethyl ether (150 mL) was added. The resulting suspension was stirred for 2 h then filtered to afford a light pink solid. This solid was washed with ethyl ether (30 mL) and dried to give the title compound (15.7 g, quantitative yield) as a TFA salt: LC-MS (APCI) *m/z* 378.2 $(M+H)^+$; ^{1}H NMR (400 MHz, DMSO-d_6) δ 11.56 (br. s., 1 H) 9.09 (s, 3 H) 7.85 (s, 1 H) 7.54 (s, 1 H) 7.09 (d, *J* = 2.32 Hz, 1 H) 4.48 (d, *J* = 6.48 Hz, 2 H) 4.11 (br. s., 1 H) 3.81 (s, 3 H) 3.46 - 3.60 (m, 1 H) 3.35 - 3.45 (m, 2 H) 3.32 (s, 3 H) 3.15 (dq, *J* = 12.01, 6.02 Hz, 1 H) 2.70 - 2.90 (m, 1 H). Absolute stereochemistry of **46** confirmed by small molecule X-ray diffraction of the crystalline HBr salt (see Supporting Information for synthesis of HBr salt)

1-{(3R,4R)-3-[5-Chloro-2-(1-methyl-1H-pyrazol-4-ylamino)-7H-pyrrolo[2,3-d]pyrimidin-4-yloxymethyl]-4-methoxy-pyrrolidin-1-yl}propenone (1) A mixture of **46** (15 g, 24.7 mmol), ethyl acetate (200 mL) and saturated aqueous $NaHCO_3$ (100 mL) was stirred at 0 °C for 10 min. Acryloyl chloride (2.3 mL, 29 mmol) was added dropwise and the resulting mixture was stirred at ambient temperature for 30 min. Ethyl acetate (150 mL) was added and the organic layer was separated. The aqueous layer was extracted with ethyl acetate (150 mL) and the combined organic layers were dried over Na_2SO_4 and evaporated to give a solid that was purified by SFC (ZymorSPHER HAP 5µ 21.2 x 150 mm column eluting with 35 % EtOH in CO_2 at 120 bar, flow 64 mL/min) to give the title compound as an off white solid (8.3 g, 78% yield): LC-MS (APCI) *m/z* 431.9 $(M+H)^+$; ^{1}H NMR (400 MHz, DMSO-d_6) δ 11.51 (s, 1 H) 9.07 (s, 1 H) 7.86 (s, 1 H) 7.52 (s, 1 H) 7.05 (s, 1 H) 6.59 (ddd, *J* = 16.75, 10.27, 1.34 Hz, 1 H) 6.14 (dd, *J* = 16.75, 2.32 Hz, 1 H) 5.68 (dt, *J* = 10.27, 2.32 Hz, 1 H) 4.44 (d, *J* = 6.24 Hz, 2 H) 3.82 - 4.09 (m, 2 H) 3.80 (s, 3 H) 3.57 - 3.76 (m, 2 H) 3.47 - 3.54 (m, 1 H) 3.31 (d, *J* = 4.65 Hz, 3 H) 2.67 - 2.92 (m, 1 H); ^{13}C NMR (asterisks denote minor rotamer peaks, 101 MHz, DMSO-d_6) δ 163.5, 162.0*, 155.6, 153.2*, 129.8, 129.4, 129.1*, 126.8*, 126.6, 123.7,120.1, 117.3, 101.9*, 101.8, 95.4*, 95.3, 81.4, 79.7*, 65.2, 65.0*, 56.3, 56.2*, 50.3, 49.7*, 46.7*, 46.2, 42.8, 41.0, 38.6.

(3*S*,4*R*)-1-Benzyl-4-methoxy-pyrrolidine-3-carboxylic acid methyl ester (**49**). To a solution of (*E*)-3-methoxy-acrylic acid methyl ester (**47**) (50 g, 431 mmol) in 2-Me-THF (600 mL) and TFA (6.7 mL) at 0 °C was added *N*-(methoxymethyl)-*N*-(trimethylsilylmethyl)-benzylamine (**48**) (204 g, 859 mmol, 2 equiv) dropwise. After addition, reaction was allowed to warm to room temperature and stirred for 2 h. Reaction was transferred to a separatory funnel, washed with saturated aqueous $NaHCO_3$, saturated aqueous NaCl, then dried over Na_2SO_4 and the solvent

was removed to leave the crude racemic product as a yellow oil which was purified over silica gel (10% – 35% EtOAc/heptane) to give the racemic *trans* product (**49**) as a yellow oil (82.7 g).

Enantiomer separation by chiral-SFC (Chiralpak AD-H 4.6 x 250 mm column 4% MeOH w/0.1 % diethylamine, 140 bar, 3.0 mL/min) gave the desired single isomer product (**50**) (34 g, 32% yield): LC-MS (APCI) *m/z* 250.0 $(M+H)^+$; ^{1}H NMR (400 MHz, DMSO-d_6) δ 7.22 - 7.39 (m, 5 H) 4.07 - 4.12 (m, 1 H) 3.66 (s, 3 H) 3.51 - 3.63 (m, 2 H) 3.23 (s, 3 H) 2.90 - 2.96 (m, 1 H) 2.82 - 2.88 (m, 1 H) 2.69 (dd, J = 9.95, 6.42 Hz, 1 H) 2.55 - 2.63 (m, 2 H); $[\alpha]_D^{27}$ = +23.8º (*c* = 1.3, MeOH).

(3*S*,4*R*)-4-Methoxy-pyrrolidine-1,3-dicarboxylic acid 1-tert-butyl ester 3-methyl ester (**51**). A solution of (3*S*,4*R*)-1-benzyl-4-methoxy-pyrrolidine-3-carboxylic acid methyl ester (**50**) (35 g, 140.4 mmol) in ethanol (500 mL) was purged with nitrogen and then $Pd(OH)_2$ (2 g, 0.1 equivalent) was added and the mixture was stirred overnight under an atmosphere of hydrogen gas at approximately 15 psi (via hydrogen balloon). The reaction was filtered through Celite® and di-*tert*-butyl dicarbonate (30.9 g, 142 mmol) was added to the resulting filtrate slowly with stirring. After one hour the reaction mixture was concentrated and the crude material was purified through a short silica gel column eluting with 10 % EtOAc/heptane for 2 volumes then 1:1 EtOAc/heptane until the product was completely eluted. Product fractions were combined and concentrated to give the title compound as a clear oil, (35.81 g, 98% yield): LC-MS (APCI) *m/z* 160.1 $(M+H)^+$ for product minus Boc group; ^{1}H NMR (400 MHz, DMSO-d_6) δ 4.06 (d, *J* = 4.78 Hz, 1 H) 3.65 (s, 3 H) 3.35 - 3.53 (m, 3 H) 3.23 - 3.28 (m, 4 H) 3.17 (br. s., 1 H) 1.39 (s, 9 H); $[\alpha]_D$= -12.5 degrees (*c* = 0.87, MeOH).

(3*R*,4*R*)-3-Hydroxymethyl-4-methoxy-pyrrolidine-1-carboxylic acid tert-butyl ester (**36**). Lithium borohydride (12.7 g, 583 mmol) was added portion wise to a solution of (3*S*,4*R*)-4-methoxy-pyrrolidine-1,3-dicarboxylic acid 1-tert-butyl ester 3-methyl ester (**51**) (35.81 g, 138 mmol) in THF (600 mL), then the reaction was heated to 60 °C for 4 h. The reaction was quenched with water at 0 °C and extracted with EtOAc. The organic layer was washed with saturated aqueous NaCl and dried over Na_2SO_4. The solvent was removed and the residue was purified through a plug of silica (3:1 EtOAc/heptane) to yield the title compound as a clear oil (29.35 g, 92% yield): LC-MS (APCI) *m/z* 132.2 $(M+H)^+$ for product minus Boc group; ^{1}H NMR (400 MHz, $CDCl_3$) δ 3.77 - 3.83 (m, 1 H) 3.50 - 3.66 (m, 4H) 3.33 (d, *J* = 4.03 Hz, 4 H) 3.19 (dd, *J* = 11.08, 5.29 Hz, 1 H) 2.37 - 2.47 (m, 1 H) 1.46 (s, 9 H); $[\alpha]_D$= +9.3 degrees (*c* = 0.86, MeOH).

Computational Modeling Methods. All molecules were prepared for docking simulation using LigPrep 2.5 (Schrödinger) to considered proper protonation states and tautomers. The docking simulation was performed with Glide 5.7 (Schrödinger) using protein models based on in-house crystal structures where Cys797 was mutated to Alanine to avoid a crash with Michael acceptor on molecules. A pharmacophore-type constraint was applied during docking to locate b-carbon of Michael acceptor in a target space for alkylation. Protein-Ligand complexes were minimized using the OPLS2005 force field.

Biochemical Kinase Assays. EGFR kinase activity assays were reported previously. Methods to estimate reversible binding affinities of covalent inhibitors are discussed in the supporting information section.

Intrinsic Chemical Reactivity Assay. The intrinsic chemical reactivity was accessed by evaluating the rate of electrophilic attack of the test compound to a strong nucleophile, glutathione (GSH). This was achieved by monitoring test compound loss during the reaction via LC-MS/MS detection. The experiment was initiated with an aliquot (100 µL) of the test compound to a reaction buffer consisting of 100 µM phosphate buffer pH 7.4, in the presence or absence of 5mM GSH. The reaction which did not contain GSH was used as a control for chemical instability. Each compound was tested experimentally in duplicate. The final test compound concentration was 1 µM. The 37°C reaction temperature was maintained throughout the entire experiment. Aliquots of the reaction volume (100 µL) were taken at 0, 5, 15, 30, 45, 60, 90, and 120 min and quenched 1:1(v:v) with 40 mM N-ethylmaleimide (NEM) in acetonitrile containing internal standard. CI-1033 was served as the positive control in all experiments.

A linear regression analysis using the natural log of the peak area ratio, based on the internal standard, versus time provided the elimination constant (k_{el}). Half-life was calculated as ln2/ -(k_{el}). The intrinsic reactivity of each test compound was reported as the ratio of the compound half-life compared to the half-life of canertinib.

Cell Lines and Culture Conditions. H1975 and A549 cancer cell lines were purchased from ATCC and were cultured according to ATCC recommendations. PC9 cells were purchased from RIKEN Cell Bank (Tsukuba, Ibaraki Prefecture, Japan) and were cultured in Gibco RPMI 1640 (Life Technologies, Carlsbad, CA, USA) medium with 10% FBS (Sigma, St. Louis, MO, USA). H3255 cells were from Dr. Bruce E. Johnson at the National Cancer Institute (Bethesda, MD, USA) and were cultured in RPMI 1640, 10% FBS, and ACL-4 supplement (Mediatech Inc, Manassas, VA, USA). PC9-DRH, harboring both the single-mutant (Del) and double-mutant (Del/T790M) alleles, is a pool of cells derived from PC9 parental line that was selected after

treatment with gradually increasing concentrations of dacomitinib up to 2 μM. PC9-DRH EGFR alleles consist of 70% Del/T790M and 30% Del. PC9-DRH cells were cultured in Gibco RPMI 1640 medium with 10% FBS, and maintained in dacomitinib (2 μM).

EGFR Cellular Autophosphorylation ELISA. Cells were plated (25,000 - 50,000 cells/well) in a final volume of 100 μL of complete media in 96-well microtiter plates and cultured overnight (37 °C, 5% CO_2). Inhibitors were solubilized in DMSO and tested in duplicate utilizing 11-point serial dilutions with the highest concentration at 1 or 10 μM (0.3% v/v final DMSO). Inhibitors were incubated with cells for 2 h at 37 °C, 5% CO_2. For EGFR wild type assays, cells were plated in full-serum (10%) media for 24 h prior to compound treatment; cells were treated in full serum media as described and then stimulated for 10 min with EGF (Life Technologies) in serum-free media (50 ng/mL for A549). For all cells post inhibitor treatment (+/- EGF), media was removed and 100 μL of ice-cold lysis buffer was added: 1x cell lysis buffer (Cell Signaling Technology, Danvers, MA, USA), 1 mM phenylmethanesulfonyl fluoride (Calbiochem/EMD Chemicals, Billerica, MA, USA), 1 mM sodium orthovanadate (New England Biolabs Inc, Ipswich, MA, USA), complete Mini EDTA-free Protease Inhibitor Cocktail Tablets (Roche Applied Science, Indianapolis, IN, USA), and PhosSTOP (Roche Applied Science). Plates were shaken (20-30 min, 4 °C) to lyse the cells and 100 μL lysate was added to an ELISA plate. PathScan Phospho-EGF Receptor (Try1068) Sandwich ELISA (Cell Signaling Technology) was used to quantify EGFR autophosphorylation per the manufacturer's protocol. IC_{50} values were determined by nonlinear regression analysis with a four-parameter fit by utilizing a Microsoft Excel-based macro.

ASSOCIATED CONTENT

Supporting information.

Methods to estimate reversible binding affinities of covalent inhibitors, experimental procedures and spectral data for compounds **14-22** and relevant intermediates, additional data on proteome wide selectivity for compound **1**, kinase selectivity data for compound **1**, ligand torsional strain energy analysis for **15** and **16**, ligand strain energy analysis for bound conformation of compound **1** in EGFR DM, and modeling of compound **10** in EGFR WT protein. This material is free of charge via the Internet at http://pubs.acs.org.

AUTHOR INFORMATION

Corresponding Authors

*E-mail: henry.cheng@pfizer.com. Phone: 858-622-3208.

*Email: sajiv.k.nair@pfizer.com. Phone: 858-526-4894.

*Email: brion.murray@pfizer.com. Phone: 858-622-6038

Notes

The authors declare no competing financial interest.

Compound **1** (PF-06459988) is commercially available via Sigma Aldrich (catalog # PZ0296).

ACKNOWLEDGMENTS

We are grateful to Klaus Dress for data management and visualization, Jeff Elleraas, Loanne Chung and Phuong Tran for purification work.

ABBREVIATIONS

EGFR, epidermal growth factor receptor; WT, wild-type; DM, double mutant (L858R/T790M, or Del/T790M); TM, triple mutant (L858R/T790M/V948R); KD, Del, exon 19 E746-A750 deletion oncogenic mutation; kinase domain; NSCLC, non-small-cell lung cancer; TKI, tyrosine kinase inhibitor; GSH, glutathione; PK, pharmacokinetics; HLM, human liver microsome, DOF, dofetilide; sol, solubility; PSA, polar surface area; RRCK, permeability measured with low-efflux MDCKII cell.

ACCESSION CODES

PDB codes are: 5HG7 for compound **1**, 5HG5 for compound **10**, 5HG8 for compound **12**, 5HG9 for compound **14**.

REFERENCES

1. Ferlay, J. S., I.; Ervik, M.; Dikshit, R.; Eser, S.; Mathers, C.; Rebelo, M.; Parkin, D. M.; Forman, D.; Bray, F. , Cancer Incidence and Mortality Worldwide: IARC CancerBase No. 11 [Internet]. *GLOBOCAN 2012 v1.1,* .

2. Ohashi, K.; Maruvka, Y. E.; Michor, F.; Pao, W., Epidermal growth factor receptor tyrosine kinase inhibitor-resistant disease. *Journal of Clinical Oncology* **2013,** *31* (8), 1070-1080.

3. Barker, A. J.; Gibson, K. H.; Grundy, W.; Godfrey, A. A.; Barlow, J. J.; Healy, M. P.; Woodburn, J. R.; Ashton, S. E.; Curry, B. J.; Scarlett, L.; Henthorn, L.; Richards, L., Studies leading to the identification of ZD1839 (iressa): an orally active, selective epidermal growth factor receptor tyrosine kinase inhibitor targeted to the treatment of cancer. *Bioorganic & Medicinal Chemistry Letters* **2001,** *11* (14), 1911-1914.
4. Shepherd, F. A.; Pereira, J. R.; Ciuleanu, T.; Tan, E. H.; Hirsh, V.; Thongprasert, S.; Campos, D.; Maoleekoonpiroj, S.; Smylie, M.; Martins, R.; van Kooten, M.; Dediu, M.; Findlay, B.; Tu, D.; Johnston, D.; Bezjk, A.; Clark, G.; Santabarbara, P.; Seymour, L., Erlotinib in previously treated non-small-cell lung cancer. *New England Journal of Medicine* **2005,** *353* (2), 123-132.
5. Lichtenberger, B. M.; Gerber, P. A.; Holcmann, M.; Buhren, B. A.; Amberg, N.; Smolle, V.; Schrumpf, H.; Boelke, E.; Ansari, P.; MacKenzie, C.; Wollenberg, A.; Kislat, A.; Fischer, J. W.; Roeck, K.; Harder, J.; Schroeder, J. M.; Homey, B.; Sibilia, M., Epidermal EGFR controls cutaneous host defense and prevents inflammation. *Sci. Transl. Med.* **2013,** *5* (199), 199ra111, 14 pp.
6. Mascia, F.; Lam, G.; Keith, C.; Garber, C.; Steinberg, S. M.; Kohn, E.; Yuspa, S. H., Genetic ablation of epidermal EGFR reveals the dynamic origin of adverse effects of anti-EGFR therapy. *Sci. Transl. Med.* **2013,** *5* (199), 199ra110, 13 pp.
7. Yu, H. A.; Arcila, M. E.; Rekhtman, N.; Sima, C. S.; Zakowski, M. F.; Pao, W.; Kris, M. G.; Miller, V. A.; Ladanyi, M.; Riely, G. J., Analysis of Tumor Specimens at the Time of Acquired Resistance to EGFR-TKI Therapy in 155 Patients with EGFR-Mutant Lung Cancers. *Clinical Cancer Research* **2013,** *19* (8), 2240-2247.
8. Kornev, A. P.; Taylor, S. S.; Ten Eyck, L. F., A helix scaffold for the assembly of active protein kinases. *Proceedings of the National Academy of Sciences of the United States of America* **2008,** *105* (38), 14377-14382,S14377/1-S14377/12.
9. Kornev, A. P.; Taylor, S. S., Defining the conserved internal architecture of a protein kinase. *Biochimica et Biophysica Acta, Proteins and Proteomics* **2010,** *1804* (3), 440-444.
10. Taylor, S. S.; Shaw, A. S.; Kannan, N.; Kornev, A. P., Integration of signaling in the kinome: Architecture and regulation of the αC Helix. *Biochimica et Biophysica Acta, Proteins and Proteomics* **2015**, Ahead of Print.
11. Barf, T.; Kaptein, A., Irreversible Protein Kinase Inhibitors: Balancing the Benefits and Risks. *Journal of Medicinal Chemistry* **2012,** *55* (14), 6243-6262.
12. Liu, Q.; Sabnis, Y.; Zhao, Z.; Zhang, T.; Buhrlage, S. J.; Jones, L. H.; Gray, N. S., Developing Irreversible Inhibitors of the Protein Kinase Cysteinome. *Chem. Biol. (Oxford, U. K.)* **2013,** *20* (2), 146-159.
13. Flanagan, M. E.; Abramite, J. A.; Anderson, D. P.; Aulabaugh, A.; Dahal, U. P.; Gilbert, A. M.; Li, C.; Montgomery, J.; Oppenheimer, S. R.; Ryder, T.; Schuff, B. P.; Uccello, D. P.; Walker, G. S.; Wu, Y.; Brown, M. F.; Chen, J. M.; Hayward, M. M.; Noe, M. C.; Obach, R. S.; Philippe, L.; Shanmugasundaram, V.; Shapiro, M. J.; Starr, J.; Stroh, J.; Che, Y., Chemical and Computational Methods for the Characterization of Covalent Reactive Groups for the Prospective Design of Irreversible Inhibitors. *Journal of Medicinal Chemistry* **2014,** *57* (23), 10072-10079.
14. Allen, L. F.; Eiseman, I. A.; Fry, D. W.; Lenehan, P. F., CI-1033, an irreversible pan-erbB receptor inhibitor and its potential application for the treatment of breast cancer. *Seminars in Oncology* **2003,** *30* (5, Suppl. 16), 65-78.
15. Engelman, J. A.; Zejnullahu, K.; Gale, C.-M.; Lifshits, E.; Gonzales, A. J.; Shimamura, T.; Zhao, F.; Vincent, P. W.; Naumov, G. N.; Bradner, J. E.; Althaus, I. W.; Gandhi, L.; Shapiro, G. I.; Nelson, J. M.; Heymach, J. V.; Meyerson, M.; Wong, K.-K.; Jaenne, P. A., PF00299804, an Irreversible Pan-ERBB Inhibitor, Is Effective in Lung Cancer Models with EGFR and ERBB2 Mutations that Are Resistant to Gefitinib. *Cancer Research* **2007,** *67* (24), 11924-11932.
16. Miller, V. A.; Hirsh, V.; Cadranel, J.; Chen, Y.-M.; Park, K.; Kim, S.-W.; Zhou, C.; Su, W.-C.; Wang, M.; Sun, Y.; Heo, D. S.; Crino, L.; Tan, E.-H.; Chao, T.-Y.; Shahidi, M.; Cong, X. J.; Lorence, R. M.; Yang, J.

C.-H., Afatinib versus placebo for patients with advanced, metastatic non-small-cell lung cancer after failure of erlotinib, gefitinib, or both, and one or two lines of chemotherapy (LUX-Lung 1): a phase 2b/3 randomised trial. *Lancet Oncology* **2012,** *13* (5), 528-538.

17. Zhou, W.; Ercan, D.; Chen, L.; Yun, C.-H.; Li, D.; Capelletti, M.; Cortot, A. B.; Chirieac, L.; Iacob, R. E.; Padera, R.; Engen, J. R.; Wong, K.-K.; Eck, M. J.; Gray, N. S.; Janne, P. A., Novel mutant-selective EGFR kinase inhibitors against EGFR T790M. *Nature (London, United Kingdom)* **2009,** *462* (7276), 1070-1074.

18. Walter, A. O.; Sjin, R. T. T.; Haringsma, H. J.; Ohashi, K.; Sun, J.; Lee, K.; Dubrovskiy, A.; Labenski, M.; Zhu, Z.; Wang, Z.; Sheets, M.; St. Martin, T.; Karp, R.; van Kalken, D.; Chaturvedi, P.; Niu, D.; Nacht, M.; Petter, R. C.; Westlin, W.; Lin, K.; Jaw-Tsai, S.; Raponi, M.; Van Dyke, T.; Etter, J.; Weaver, Z.; Pao, W.; Singh, J.; Simmons, A. D.; Harding, T. C.; Allen, A., Discovery of a Mutant-Selective Covalent Inhibitor of EGFR that Overcomes T790M-Mediated Resistance in NSCLC. *Cancer Discovery* **2013,** *3* (12), 1404-1415.

19. Cross, D. A. E.; Ashton, S. E.; Ghiorghiu, S.; Eberlein, C.; Nebhan, C. A.; Spitzler, P. J.; Orme, J. P.; Finlay, M. R. V.; Ward, R. A.; Mellor, M. J.; Hughes, G.; Rahi, A.; Jacobs, V. N.; Brewer, M. R.; Ichihara, E.; Sun, J.; Jin, H.; Ballard, P.; Al-Kadhimi, K.; Rowlinson, R.; Klinowska, T.; Richmond, G. H. P.; Cantarini, M.; Kim, D.-W.; Ranson, M. R.; Pao, W., AZD9291, an Irreversible EGFR TKI, Overcomes T790M-Mediated Resistance to EGFR Inhibitors in Lung Cancer. *Cancer Discovery* **2014,** *4* (9), 1046-1061.

20. Finlay, M. R. V.; Anderton, M.; Ashton, S.; Ballard, P.; Bethel, P. A.; Box, M. R.; Bradbury, R. H.; Brown, S. J.; Butterworth, S.; Campbell, A.; Chorley, C.; Colclough, N.; Cross, D. A. E.; Currie, G. S.; Grist, M.; Hassall, L.; Hill, G. B.; James, D.; James, M.; Kemmitt, P.; Klinowska, T.; Lamont, G.; Lamont, S. G.; Martin, N.; McFarland, H. L.; Mellor, M. J.; Orme, J. P.; Perkins, D.; Perkins, P.; Richmond, G.; Smith, P.; Ward, R. A.; Waring, M. J.; Whittaker, D.; Wells, S.; Wrigley, G. L., Discovery of a Potent and Selective EGFR Inhibitor (AZD9291) of Both Sensitizing and T790M Resistance Mutations That Spares the Wild Type Form of the Receptor. *Journal of Medicinal Chemistry* **2014,** *57* (20), 8249-8267.

21. Ward, R. A.; Anderton, M. J.; Ashton, S.; Bethel, P. A.; Box, M.; Butterworth, S.; Colclough, N.; Chorley, C. G.; Chuaqui, C.; Cross, D. A. E.; Dakin, L. A.; Debreczeni, J. E.; Eberlein, C.; Finlay, M. R. V.; Hill, G. B.; Grist, M.; Klinowska, T. C. M.; Lane, C.; Martin, S.; Orme, J. P.; Smith, P.; Wang, F.; Waring, M. J., Structure- and Reactivity-Based Development of Covalent Inhibitors of the Activating and Gatekeeper Mutant Forms of the Epidermal Growth Factor Receptor (EGFR). *Journal of Medicinal Chemistry* **2013,** *56* (17), 7025-7048.

22. Chang, S.; Zhang, L.; Xu, S.; Luo, J.; Lu, X.; Zhang, Z.; Xu, T.; Liu, Y.; Tu, Z.; Xu, Y.; Ren, X.; Geng, M.; Ding, J.; Pei, D.; Ding, K., Design, Synthesis, and Biological Evaluation of Novel Conformationally Constrained Inhibitors Targeting Epidermal Growth Factor Receptor Threonine790 → Methionine790 Mutant. *Journal of Medicinal Chemistry* **2012,** *55* (6), 2711-2723.

23. Xu, S.; Xu, T.; Zhang, L.; Zhang, Z.; Luo, J.; Liu, Y.; Lu, X.; Tu, Z.; Ren, X.; Ding, K., Design, Synthesis, and Biological Evaluation of 2-Oxo-3,4-dihydropyrimido[4,5 d]pyrimidinyl Derivatives as New Irreversible Epidermal Growth Factor Receptor Inhibitors with Improved Pharmacokinetic Properties. *Journal of Medicinal Chemistry* **2013,** *56* (21), 8803-8813.

24. Zhou, W.; Liu, X.; Tu, Z.; Zhang, L.; Xin, K.; Bai, F.; Zhao, Z.; Xu, Y.; Ding, K.; Li, H., Discovery of Pteridin-7(8H)one-Based Irreversible Inhibitors Targeting the Epidermal Growth Factor Receptor (EGFR) Kinase T790M/L858R Mutant. *Journal of Medicinal Chemistry* **2013,** *56* (20), 7821-7837.

25. Xia, G.; Chen, W.; Zhang, J.; Shao, J.; Zhang, Y.; Huang, W.; Zhang, L.; Qi, W.; Sun, X.; Li, B.; Xiang, Z.; Ma, C.; Xu, J.; Deng, H.; Li, Y.; Li, P.; Miao, H.; Han, J.; Liu, Y.; Shen, J.; Yu, Y., A Chemical Tuned Strategy to Develop Novel Irreversible EGFR-TK Inhibitors with Improved Safety and Pharmacokinetic Profiles. *Journal of Medicinal Chemistry* **2014,** *57* (23), 9889-9900.

26. Engel, J.; Richters, A.; Getlik, M.; Tomassi, S.; Keul, M.; Termathe, M.; Lategahn, J.; Becker, C.; Mayer-Wrangowski, S.; Gruetter, C.; Uhlenbrock, N.; Kruell, J.; Schaumann, N.; Eppmann, S.; Kibies, P.; Hoffgaard, F.; Heil, J.; Menninger, S.; Ortiz-Cuaran, S.; Heuckmann, J. M.; Tinnefeld, V.; Zahedi, R. P.; Sos, M. L.; Schultz-Fademrecht, C.; Thomas, R. K.; Kast, S. M.; Rauh, D., Targeting Drug Resistance in EGFR

with Covalent Inhibitors: A Structure-Based Design Approach. *Journal of Medicinal Chemistry* **2015,** *58* (17), 6844-6863.

27. Cheng, H.; Johnson, T. O., Jr.; Kath, J. C.; Liu, K. K.-C.; Lunney, E. A.; Nagata, A.; Nair, S. K.; Planken, S. P.; Sutton, S. C. Preparation of pyrrolopyrimidine and purine derivatives for the treatment of abnormal cell growth. WO2013042006.

28. Planken, S.; Nair, S. K.; Kath, J. C.; Lafontaine, J.; Weinrich, S.; Cheng, H. K.; Sutton, S. C.; Johnson, T. O.; Zientek, M.; Nagata, A.; Gajiwala, K.; Solowiej, J.; Murray, B. W.; Yin, M.-J.; Hemkens, M., Discovery and development of a series of irreversible EGFR_T790M 7H-pyrrolo[2, 3-d]pyrimidine inhibitors with high selectivity over EGFR wild type. *Abstracts of Papers, 249th ACS National Meeting & Exposition, Denver, CO, United States, March 22-26, 2015* **2015**, MEDI-320.

29. Schwartz, P. A.; Kuzmic, P.; Solowiej, J.; Bergqvist, S.; Bolanos, B.; Almaden, C.; Nagata, A.; Ryan, K.; Feng, J.; Dalvie, D.; Kath, J. C.; Xu, M.; Wani, R.; Murray, B. W., Covalent EGFR inhibitor analysis reveals importance of reversible interactions to potency and mechanisms of drug resistance. *Proceedings of the National Academy of Sciences of the United States of America* **2014,** *111* (1), 173-178.

30. Kuzmic, P., Program DYNAFIT for the analysis of enzyme kinetic data: application to HIV proteinase. *Analytical Biochemistry* **1996,** *237* (2), 260-273.

31. Kuzmic, P., DynaFit - a software package for enzymology. *Methods Enzymol.* **2009,** *467* (Computer Methods, Part B), 247-280.

32. Gajiwala, K. S.; Feng, J.; Ferre, R.; Ryan, K.; Brodsky, O.; Weinrich, S.; Kath, J. C.; Stewart, A., Insights into the Aberrant Activity of Mutant EGFR Kinase Domain and Drug Recognition. *Structure (Oxford, U. K.)* **2013,** *21* (2), 209-219.

33. Di, L.; Whitney-Pickett, C.; Umland, J. P.; Zhang, H.; Zhang, X.; Gebhard, D. F.; Lai, Y.; Federico, J. J.; Davidson, R. E.; Smith, R.; Reyner, E. L.; Lee, C.; Feng, B.; Rotter, C.; Varma, M. V.; Kempshall, S.; Fenner, K.; El-kattan, A. F.; Liston, T. E.; Troutman, M. D., Development of a new permeability assay using low-efflux MDCKII cells. *Journal of Pharmaceutical Sciences* **2011,** *100* (11), 4974-4985.

34. Varma, M. V.; Gardner, I.; Steyn, S. J.; Nkansah, P.; Rotter, C. J.; Whitney-Pickett, C.; Zhang, H.; Di, L.; Cram, M.; Fenner, K. S.; El-Kattan, A. F., pH-Dependent solubility and permeability criteria for provisional biopharmaceutics classification (BCS and BDDCS) in early drug discovery. *Molecular Pharmaceutics* **2012,** *9* (5), 1199-1212.

35. Cui, J. J.; McTigue, M.; Nambu, M.; Tran-Dube, M.; Pairish, M.; Shen, H.; Jia, L.; Cheng, H.; Hoffman, J.; Le, P.; Jalaie, M.; Goetz, G. H.; Koenig, M.; Vojkovsky, T.; Zhang, F.-J.; Do, S.; Botrous, I.; Ryan, K.; Grodsky, N.; Deng, Y.-l.; Parker, M.; Timofeevski, S.; Murray, B. W.; Yamazaki, S.; Aguirre, S.; Li, Q.; Zou, H.; Christensen, J., Discovery of a Novel Class of Exquisitely Selective Mesenchymal-Epithelial Transition Factor (c-MET) Protein Kinase Inhibitors and Identification of the Clinical Candidate 2-(4-(1-(Quinolin-6-ylmethyl)-1H-[1,2,3]triazolo[4,5-b]pyrazin-6-yl)-1H-pyrazol-1-yl)ethanol (PF-04217903) for the Treatment of Cancer. *Journal of Medicinal Chemistry* **2012,** *55* (18), 8091-8109.

36. Chein, R.-J.; Corey, E. J., Strong Conformational Preferences of Heteroaromatic Ethers and Electron Pair Repulsion. *Org. Lett.* **2010,** *12* (1), 132-135.

37. Perola, E.; Charifson, P. S., Conformational Analysis of Drug-Like Molecules Bound to Proteins: An Extensive Study of Ligand Reorganization upon Binding. *Journal of Medicinal Chemistry* **2004,** *47* (10), 2499-2510.

38. Lanning, B. R.; Whitby, L. R.; Dix, M. M.; Douhan, J.; Gilbert, A. M.; Hett, E. C.; Johnson, T. O.; Joslyn, C.; Kath, J. C.; Niessen, S.; Roberts, L. R.; Schnute, M. E.; Wang, C.; Hulce, J. J.; Wei, B.; Whiteley, L. O.; Hayward, M. M.; Cravatt, B. F., A road map to evaluate the proteome-wide selectivity of covalent kinase inhibitors. *Nat. Chem. Biol.* **2014,** *10* (9), 760-767.

39. Rostovtsev, V. V.; Green, L. G.; Fokin, V. V.; Sharpless, K. B., A stepwise Huisgen cycloaddition process: copper(I)-catalyzed regioselective "ligation" of azides and terminal alkynes. *Angew. Chem., Int. Ed.* **2002,** *41* (14), 2596-2599.

40. Muchowski, J. M.; Solas, D. R., Protecting groups for the pyrrole and indole nitrogen atom. The [2-(trimethylsilyl)ethoxy]methyl moiety. Lithiation of 1-[[2-(trimethylsilyl)ethoxy]methyl]pyrrole. *J. Org. Chem.* **1984**, 49 (1), 203-5.

For Table of Content Graphic:

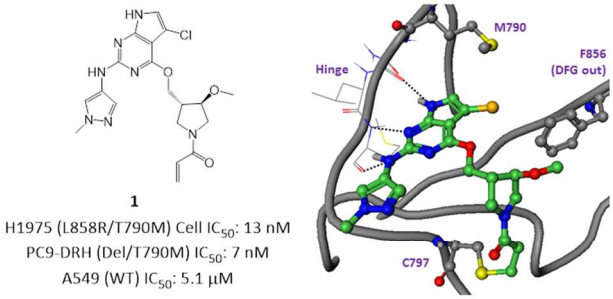

1

H1975 (L858R/T790M) Cell IC_{50}: 13 nM
PC9-DRH (Del/T790M) IC_{50}: 7 nM
A549 (WT) IC_{50}: 5.1 μM

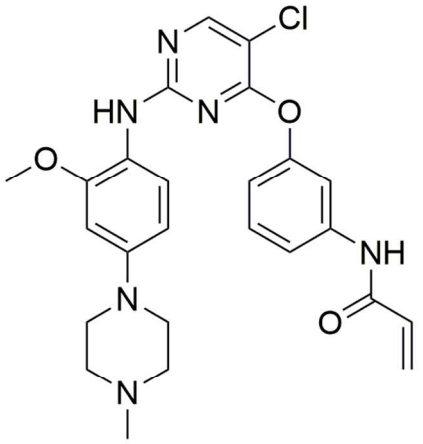

7 (WZ-4002)

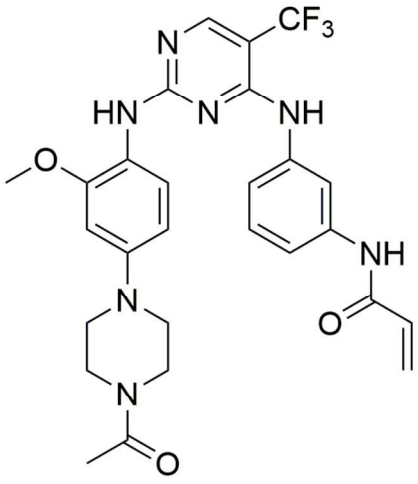

8 (CO-1868)

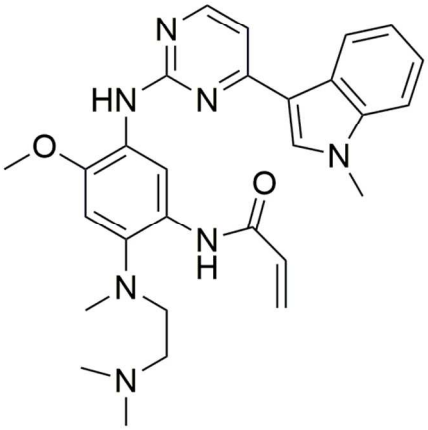

9 (AZD9291)

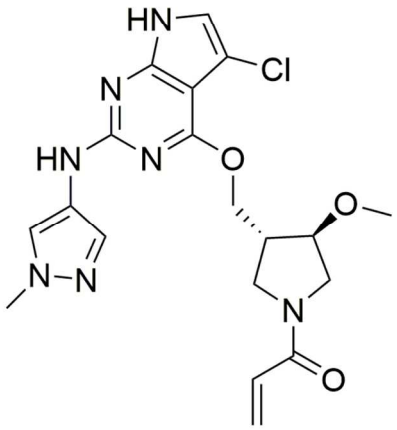

1 (PF-06459988)

108x129mm (300 x 300 DPI)

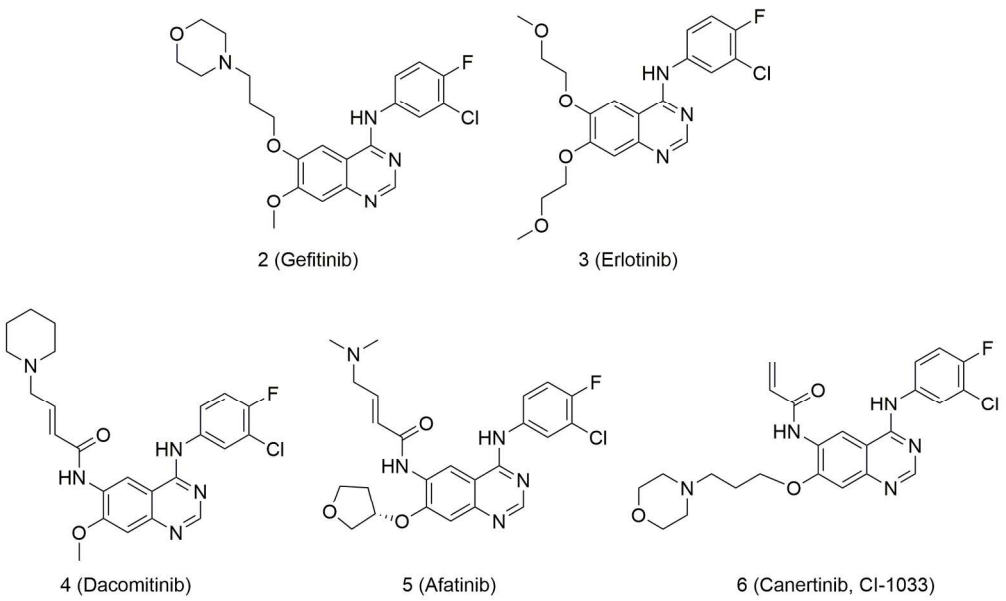

181x108mm (300 x 300 DPI)

$$E + I \underset{k_{off}}{\overset{k_{on}}{\rightleftharpoons}} E \cdot I \xrightarrow{k_{inact}} E\text{–}I$$

$$K_i = \frac{k_{off}}{k_{on}}$$

254x190mm (96 x 96 DPI)

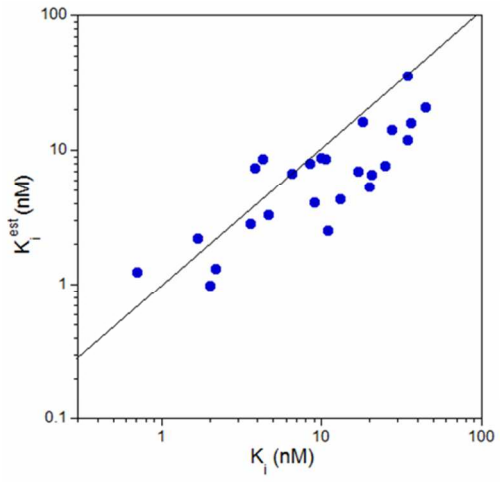

254x190mm (96 x 96 DPI)

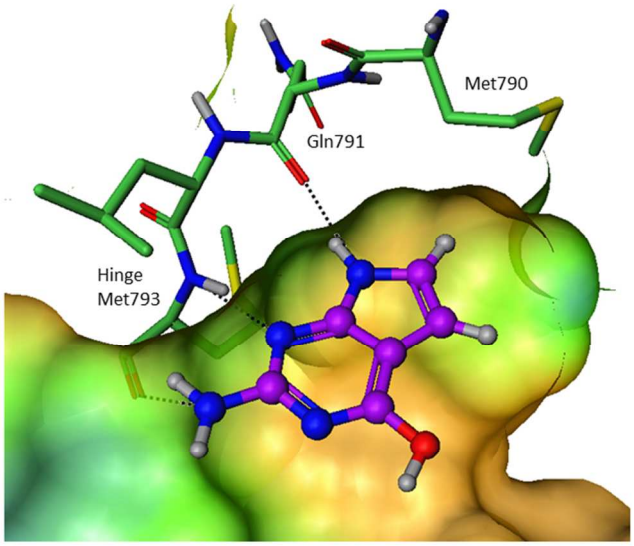

254x190mm (96 x 96 DPI)

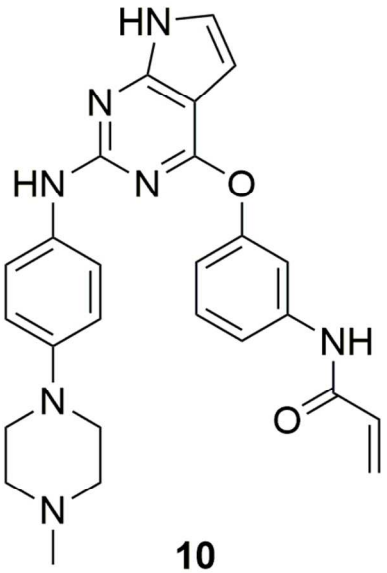

10

Kiest (DM): 2 nM
kobs/I: 51,300 M-1S-1
H1975 pEGFR IC50: 4 nM
A540 pEGFR IC50: 0.79 mM

93x55mm (300 x 300 DPI)

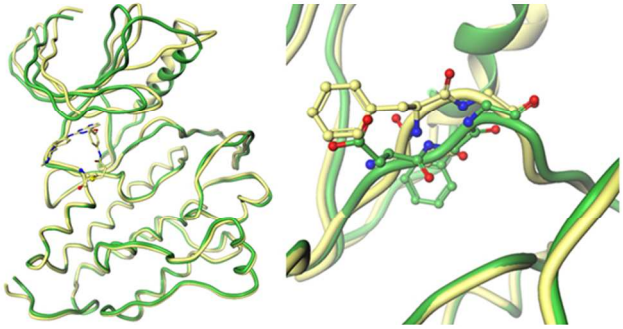

254x190mm (96 x 96 DPI)

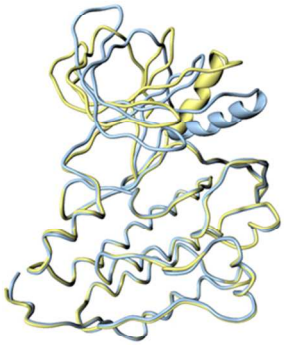

254x190mm (96 x 96 DPI)

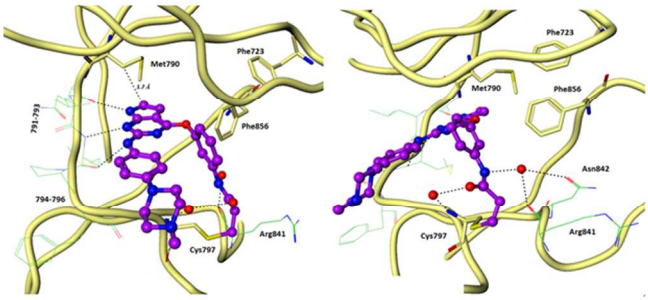

254x190mm (96 x 96 DPI)

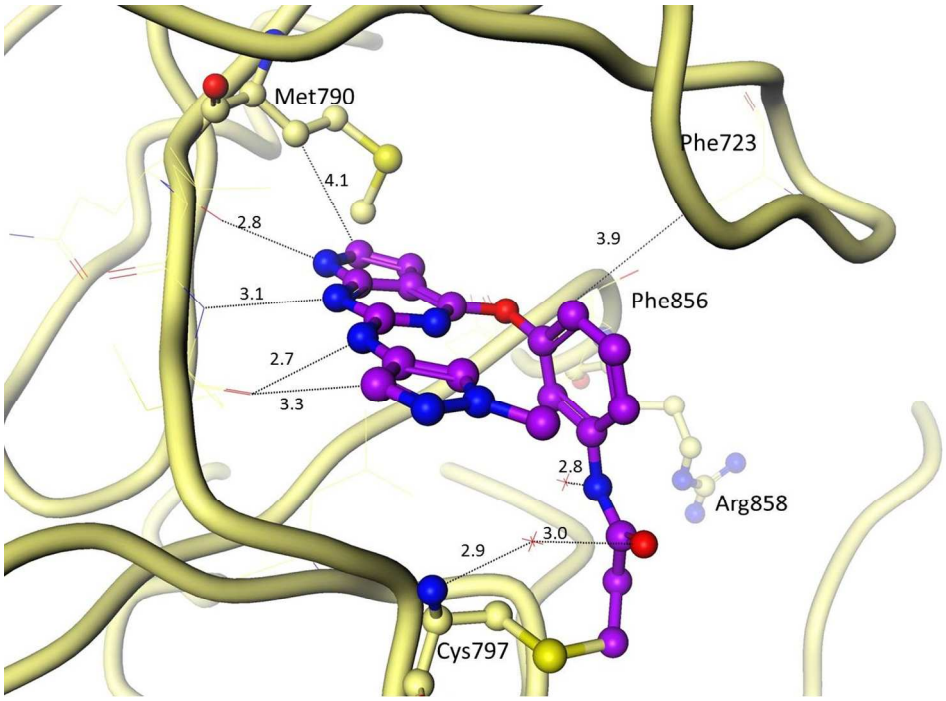

254x175mm (150 x 150 DPI)

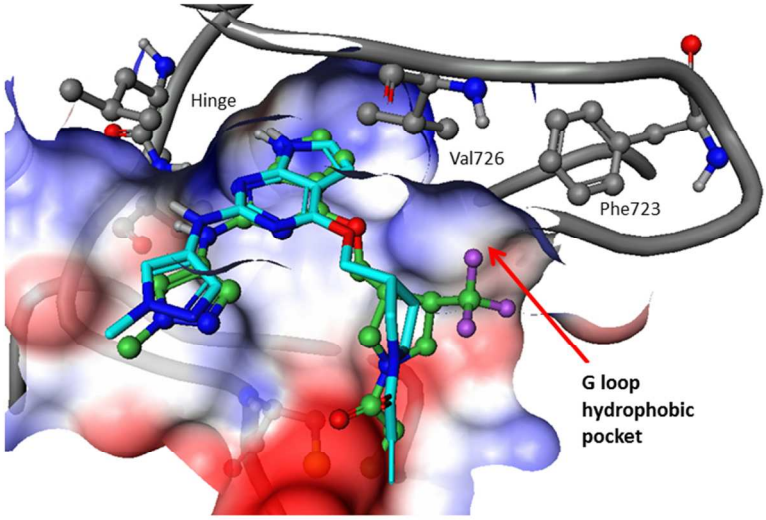

254x190mm (96 x 96 DPI)

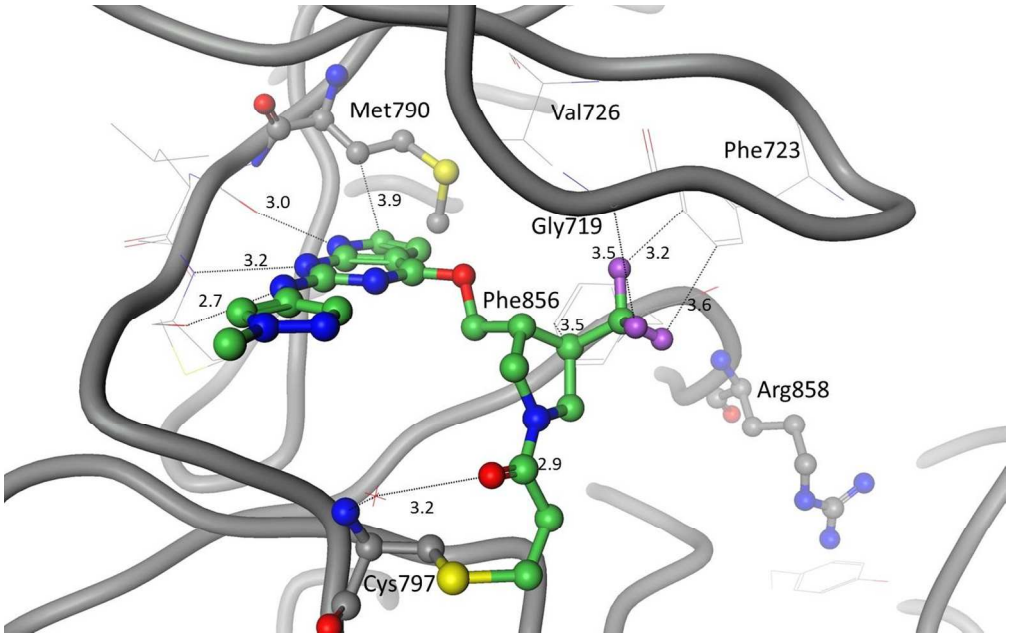

254x159mm (150 x 150 DPI)

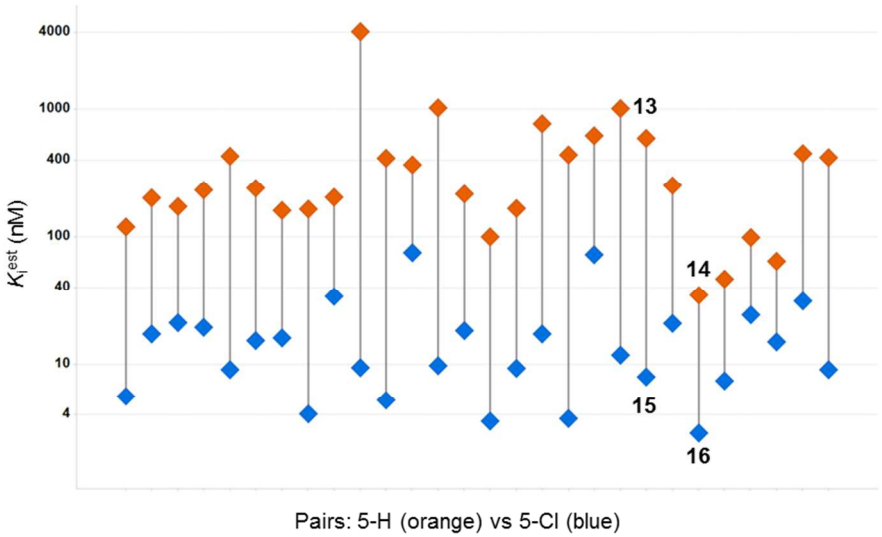

254x190mm (96 x 96 DPI)

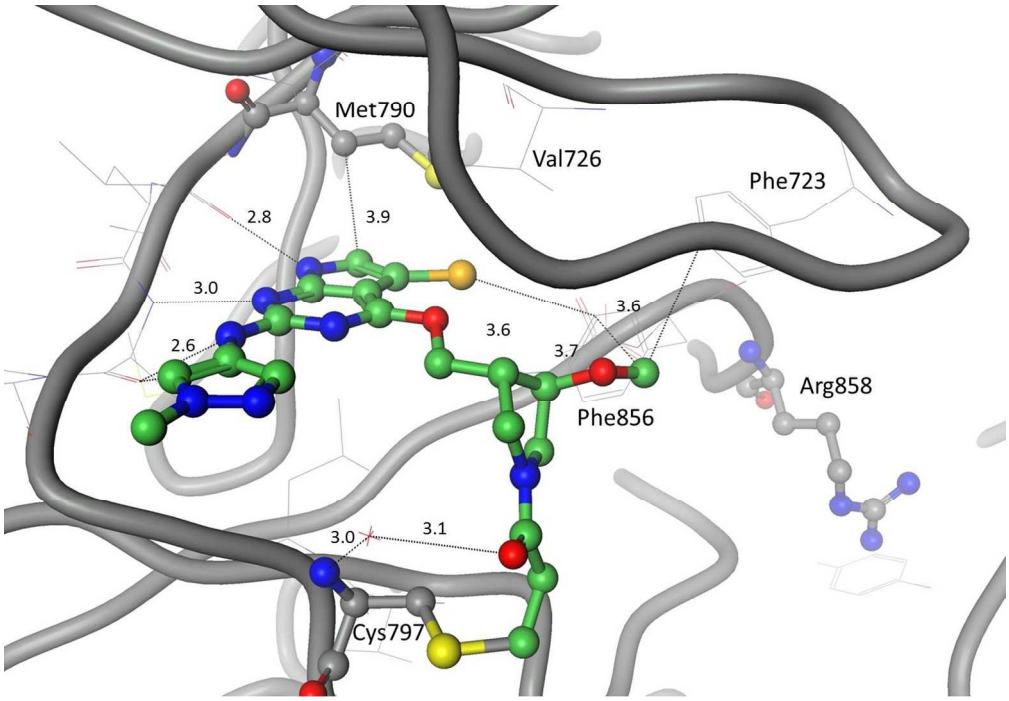

254x175mm (150 x 150 DPI)

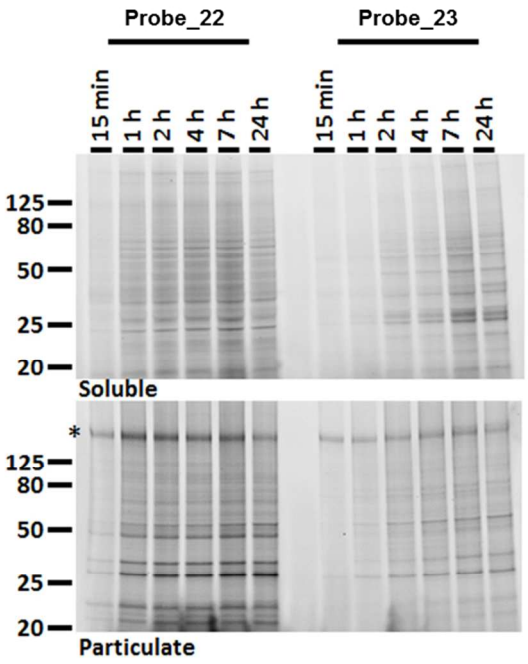

254x190mm (96 x 96 DPI)

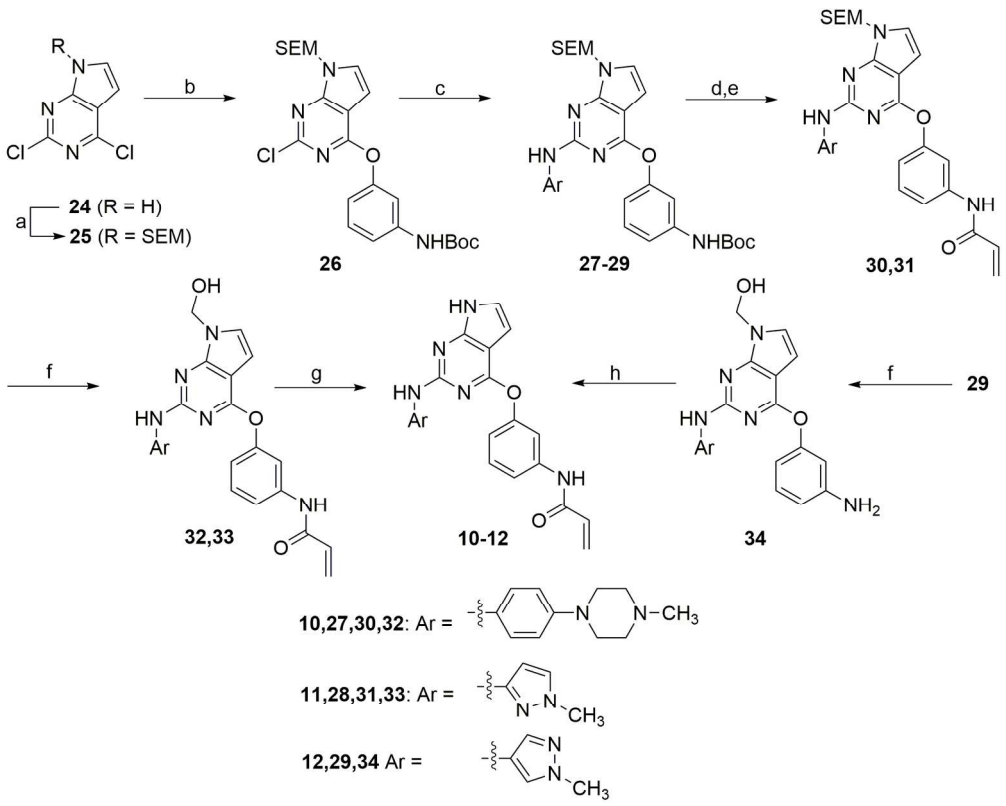

176x141mm (300 x 300 DPI)

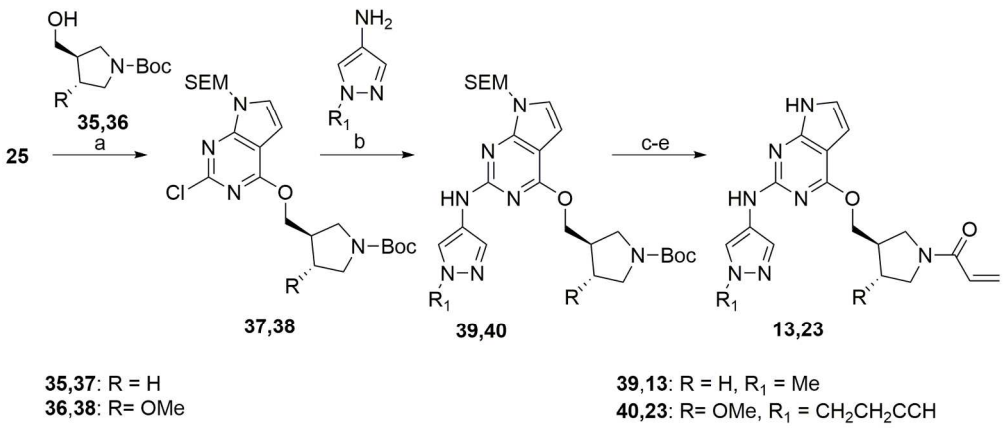

171x73mm (300 x 300 DPI)

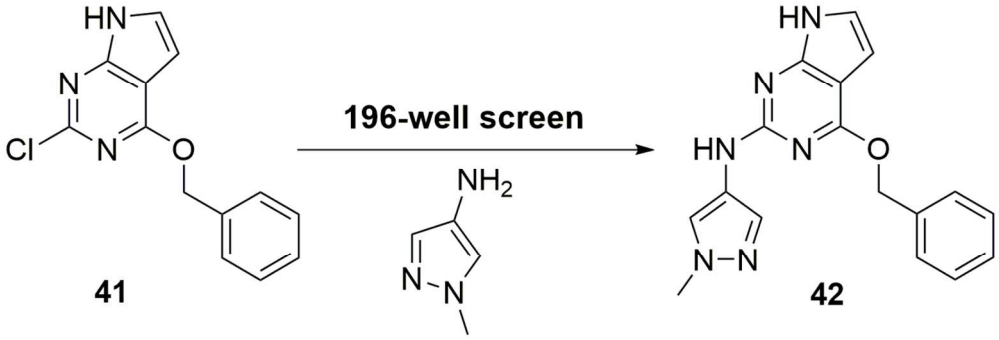

115x39mm (300 x 300 DPI)

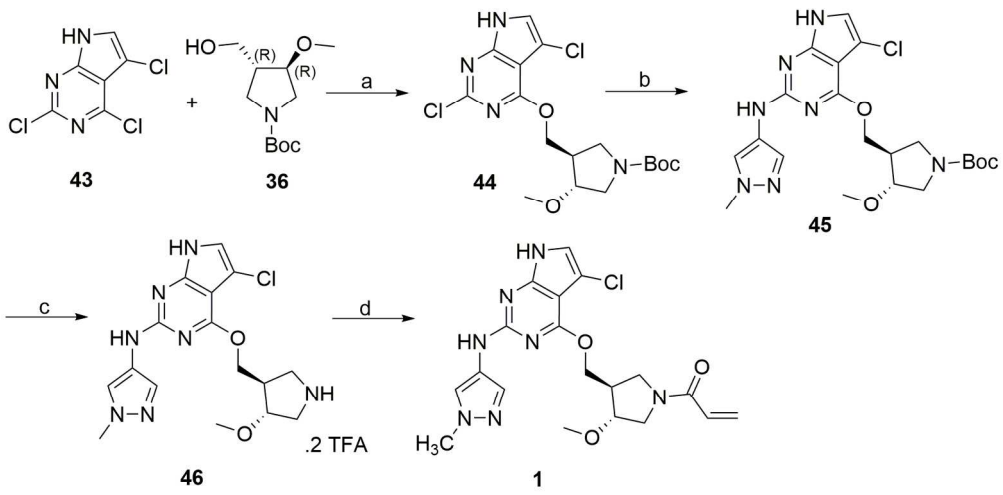

167x82mm (300 x 300 DPI)

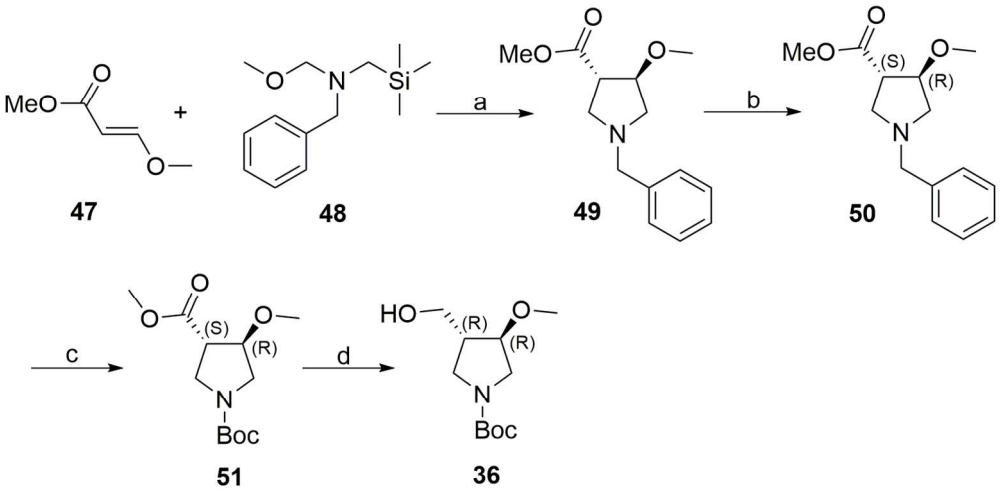

141x70mm (300 x 300 DPI)

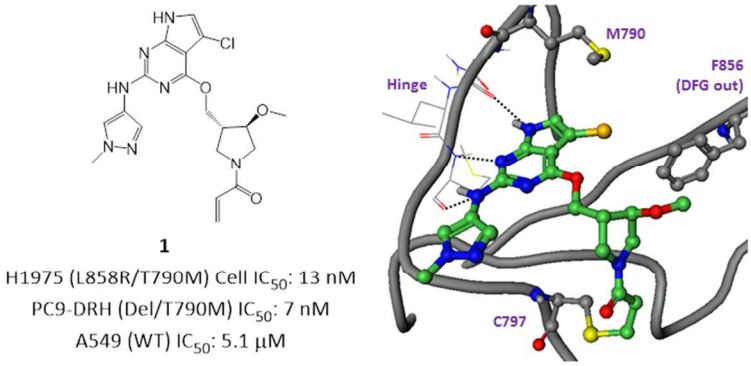

1

H1975 (L858R/T790M) Cell IC_{50}: 13 nM
PC9-DRH (Del/T790M) IC_{50}: 7 nM
A549 (WT) IC_{50}: 5.1 μM

254x190mm (96 x 96 DPI)